

Qubits with electrons on liquid helium

M. I. Dykman,^{1,*} P. M. Platzman,² and P. Seddighrad¹

¹*Department of Physics and Astronomy, Michigan State University, East Lansing, Michigan 48824*

²*Bell Laboratories, Lucent Technologies, Murray Hill, New Jersey 07974*

(Received 28 August 2002; published 3 April 2003)

We study dissipation effects for electrons on the surface of liquid helium, which may serve as the qubits of a quantum computer. Each electron is localized in a 3D potential well formed by the image potential in helium and the potential from a submicron electrode submerged into helium. We estimate parameters of the confining potential and characterize the electron energy spectrum. Decay of the excited electron state is due to two-rippylon scattering and to scattering by phonons in helium. We identify mechanisms of coupling to phonons. An estimate of contributions from different scattering mechanisms shows that the decay rate should be $\lesssim 10^4 \text{ s}^{-1}$. We analyze dephasing of the electron states due to quasielastic ripplon scattering off an electron. The dephasing rate is $\lesssim 10^2 \text{ s}^{-1}$ for $T=10 \text{ mK}$ and depends on temperature as T^3 . Decay and decoherence of the electron states result also from classical and quantum electrode noise. We relate the corresponding relaxation rates to the power spectrum of the fluctuating electric field on the electron. The dependence of the rates on the electrode parameters is obtained.

DOI: 10.1103/PhysRevB.67.155402

PACS number(s): 03.67.Lx, 73.21.-b, 76.60.Es, 73.63.-b

I. INTRODUCTION

Much interest has attracted recently the idea of creating a condensed-matter based quantum computer (QC). A major challenge is to have a system that would have a sufficiently long relaxation time, and nevertheless could be controlled with high precision and allow its quantum state to be measured. The proposed systems include localized electron spins in semiconductor heterostructures,¹⁻³ nuclear spins of ³¹P donors⁴ or ²⁹Si nuclei⁵ in a zero nuclear spin ²⁸Si matrix, electron states in a quantum dot excited by terahertz radiation,⁶ excitons in quantum dots,^{7,8} Josephson-junction based systems,⁹⁻¹⁴ electrons on helium surface,^{15,16} quantum dots coupled via a linear support,¹⁷ and trapped polar molecules.¹⁸

The system of electrons on the surface of superfluid ⁴He is in several respects attractive for making a scalable quantum computer. First, many properties of this system are already known experimentally and well understood theoretically.¹⁹ Second, electrons on helium have extremely long relaxation time: they display the highest mobility known in a condensed-matter system.²⁰ Last but not least, the typical interelectron distance is comparatively large, $\sim 1 \mu\text{m}$. To make a QC we suggested^{15,16} to fabricate a system of microelectrodes, which would be submerged beneath the helium surface. Each electrode is supposed to localize one electron above it, as seen in Fig. 1, and to control this electron. Respectively, the interelectrode distance should be $\sim 1 \mu\text{m}$, which makes fabrication technologically feasible.

The two states of an electron qubit are the two lowest states of quantized motion transverse to the surface. To further slow down the already slow relaxation, we initially proposed to apply a magnetic field B_{\perp} normal to the surface. Then the estimated relaxation time T_2 due to ripplon scattering becomes as long as 10^{-4} s , for typical $B_{\perp} \sim 1.5 \text{ T}$ and temperatures $T \approx 10 \text{ mK}$, whereas the clock frequency of the computer Ω can be in the GHz range. This attracted attention of experimentalists to the project.²¹⁻²³

In this paper we show that, even without a magnetic field, the relaxation rate of a confined electron can be much less than that of a free electrons. The rate of ripplon-induced dephasing can be even smaller than the previous estimate for a strong magnetic field. This is due to large level spacing in a 3D confining potential formed by a localizing microelectrode provided the electrode is sufficiently thin. Electrodes of an appropriate shape have already been fabricated.²²

For low temperatures, the major known dissipation mechanism is scattering by surface capillary waves, ripples. These waves are very slow. Therefore, a large distance between electron energy levels makes it impossible to conserve energy and momentum in a one-rippylon decay process. Decay of the excited electron state, i.e. electron energy relaxation may occur via scattering into two short-wavelength ripples. We show that a very important role is played also by decay processes where the electron energy goes to phonons

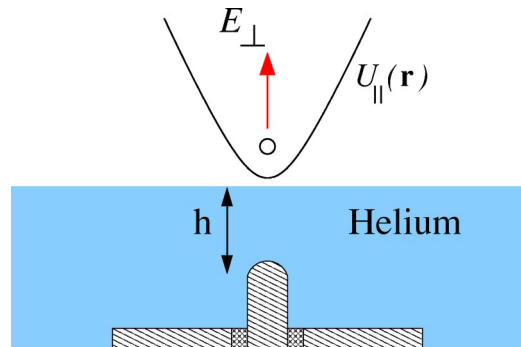


FIG. 1. (Color online) A sketch of a microelectrode submerged by the depth $h \sim 0.5 \mu\text{m}$ beneath the helium surface, with an electron localized above it. The electron is driven by a field E_{\perp} normal to the surface. This field comes from the electrode and the parallel-plate capacitor (only the lower plate of the capacitor is shown). The in-plane electron potential $U_{\parallel}(\mathbf{r})$ is parabolic near the minimum, with curvature determined by the electrode potential ($\mathbf{r}=(x,y)$ is the in-plane position vector).

in helium. The relevant phonons propagate nearly normal to the surface. We find the mechanisms of electron-phonon coupling and analyze their contribution to the decay rate.

Electron coupling to excitations in helium leads also to dephasing, i.e. to randomization of the phase difference between the electron states. The dephasing is due primarily to scattering of thermally excited riplons off an electron. We find its temperature dependence for different coupling mechanisms. We also investigate the spectrum of sideband absorption in which a microwave-induced electron transition is accompanied by creation or annihilation of a ripplon, and analyze the related decrease of the intensity of the zero-riplon absorption line.

An important problem for electrons on helium, as well as for several other proposed realizations of qubits, is noise from controlling electrodes. If the size of a qubit is small compared to the distance to the electrode, as in the case of electrons on helium, the effect of coupling to the electrode on qubit relaxation can be described in terms of the power spectrum of the fluctuating electric field of the electrode. This electric field is due to quantum electrode charge-density fluctuations. We find its power spectrum for a simple but realistic model of an electrode. This makes it possible to estimate the relaxation rate and to find how it depends on the parameters of the electrodes and the circuit.

In Sec. II below we analyze the energy spectrum of a confined electron and discuss many-electron effects. In Sec. III we discuss energy relaxation rate for different mechanisms of electron-riplon and electron-phonon coupling. In Sec. IV we consider dephasing rate. Section V deals with one-riplon sidebands and the Debye-Waller type factor in the zero-riplon absorption line. In Sec. VI we discuss electron relaxation and dephasing from fluctuations in the underlying electrodes. Section VII contains concluding remarks.

II. ELECTRON STATES IN ONE- AND MANY-ELECTRON SYSTEMS

A. Single-electron energy spectrum

The quantum computer considered in this paper is based on a set of electrons which reside in potential wells in free space above liquid helium, cf. Fig. 1. The electrons are prevented from penetrating into helium by a high potential barrier ~ 1 eV at the helium surface. For one electron, the potential well is formed by the electrostatic image in helium, the potential from the electrode, and also the potential created by the grounded plate and a parallel plate above the electron layer (the latter is not shown in Fig. 1).

We assume that the helium occupies the half space $z \leq 0$. The image potential for an electron is $-\Lambda/z$, where $\Lambda = (\epsilon - 1)e^2/4(\epsilon + 1)$, with $\epsilon \approx 1.057$ being the dielectric constant of helium. The energy spectrum for 1D motion in such a potential is hydrogenic,

$$E_n = -R/n^2 (n = 1, 2, \dots), \quad R = \Lambda^2 m / 2\hbar^2. \quad (1)$$

The effective Rydberg energy R is ≈ 8 K, and the effective Bohr radius is $r_B = \hbar^2 / \Lambda m \approx 76 \text{ \AA}$ (m is the electron mass).

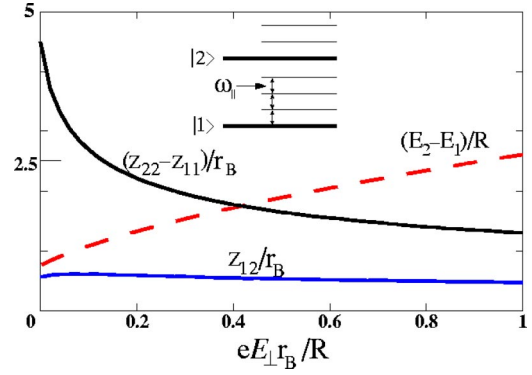


FIG. 2. (Color online) Energy difference $E_2 - E_1$ and matrix elements $z_{nm} = \langle n|z|m\rangle$ of the electron coordinate z normal to helium surface on the wave functions of the ground and first-excited states of z motion, $|1\rangle$ and $|2\rangle$, vs the overall pressing field E_\perp . The field E_\perp includes the electrode field \mathcal{E}_\perp and the field from the capacitor; $eE_\perp r_B/R = 1$ for $E_\perp \approx 0.91$ kV/cm. The inset shows the full energy level diagram. Each level E_n of z motion gives rise to a set of energy levels of vibrations parallel to helium surface, with typical spacing $\hbar\omega_\parallel$.

The electrode potential leads to Stark shift of the energy levels $(1)^{24}$ and to quantization of motion parallel to the surface. A realistic estimate of this potential and of the electron energy spectrum can be made by modeling the electrode as a conducting sphere with a diameter $2r_{el}$ equal to the electrode diameter. The center of the sphere is located at depth h beneath the helium surface. Typically we expect h to be $\sim 0.5 \mu\text{m}$, so that it largely exceeds the distance from the electron to the surface $\sim r_B$. For $z \ll h$ and for the in-plane distance from the electrode $r = (x^2 + y^2)^{1/2} \ll h, (h^2 - r_{el}^2)^{1/2}$, the electron potential energy is

$$U(\mathbf{r}, z) \approx -\frac{\Lambda}{z} + e\mathcal{E}_\perp z + \frac{1}{2}m\omega_\parallel^2 r^2 \quad (2)$$

with

$$\mathcal{E}_\perp = V_{el} r_{el} h^{-2} + e r_{el} h (h^2 - r_{el}^2)^{-2},$$

$$\omega_\parallel = (e\mathcal{E}_\perp / mh)^{1/2}. \quad (3)$$

Here, $\mathbf{r} = (x, y)$ is the electron in-plane position vector, and V_{el} is the electrode potential. The second term in \mathcal{E}_\perp comes from the image of the electron in the spherical electrode.

In approximation (2), the electron out-of-plane and in-plane motions separate, with in-plane motion being just harmonic oscillations. Variational calculations of the energy spectrum of the out-of-plane motion were done earlier.²⁴ The simple model (2) with an infinite wall at $z = 0$ describes the observed transition frequencies with an error of only a few percent, which is sufficient for the present purposes (more realistic models have been discussed in literature, see Refs. 25–27 and papers cited therein). The full electron energy spectrum in potential (2) is sketched in the inset of Fig. 2. The two states of a qubit are the ground and first-excited states of motion transverse to the surface, $|1\rangle$ and $|2\rangle$, both corresponding to the ground state of in-plane vibrations.

In what follows, we characterize the electron state $|i, \nu, m_\nu\rangle$ with the following three quantum numbers: $i=1, 2$ enumerates the state of out-of-plane motion, $\nu=0, 1, \dots$ gives the energy level of in-plane vibrations, and $m_\nu=0, 1, \dots, \nu$ enumerates degenerate vibrational states within this level. In calculations of the relaxation parameters we will assume that in-plane and out-of-plane motions can be separated, so that

$$|i, \nu, m_\nu\rangle = |i\rangle |\nu, m_\nu\rangle$$

with $|i\rangle$ and $|\nu, m_\nu\rangle$ being functions of z and \mathbf{r} , respectively.

B. Choosing parameters of the many-electron system

1. Working frequency considerations

For a multiqubit multielectrode QC, the depth h by which the controlling electrodes are submerged into helium, the interelectrode distances d_{ij} , and the electrode potentials should be chosen in such a way that would optimize performance of the QC. This includes, in the first place, having a high working frequency Ω_{QC} and low relaxation rate Γ . The frequency Ω_{QC} is limited by the rate of single-qubit operations and by the rate of excitation transfer between neighboring qubits, which is determined by the qubit-qubit interaction.

Single-qubit operations will be performed¹⁵ by applying pulses of resonant microwave radiation, which cause transitions between the states $|1\rangle$ and $|2\rangle$. The corresponding Rabi frequency is $\Omega_R = e\mathcal{E}_m |z_{12}|/\hbar$, where \mathcal{E}_m is the field amplitude. As seen from Fig. 2, $|z_{12}|/r_B \gtrsim 0.5$, and therefore even a comparatively weak field $\mathcal{E}_m = 1$ V/cm gives $\Omega_R \gtrsim 6 \times 10^8$ s⁻¹. This shows that single-qubit operations should not limit Ω_{QC} at least at the level of $10^7 - 10^8$ Hz.

Because the wave functions of different electrons do not overlap, the interaction between the qubits that we consider is dipolar, as in liquid-state NMR quantum computers.²⁸ An important feature of electrons on helium is that their localization length normal to the surface r_B greatly exceeds the atomic radius, which makes the dipole-dipole interaction orders of magnitude stronger than the dipolar interaction in atomic systems.

Of interest to us is the part of the qubit-qubit interaction that depends on the states of the qubits. Two types of dipole moments have to be distinguished. One is determined by the difference $z_{11} - z_{22}$ of average distances of the electron from helium surface in the states $|1\rangle$ and $|2\rangle$. The dipole moment $e(z_{11} - z_{22})$ does not depend on time, if we take into account time dependence of the wave functions, it can be called “static.” The interaction energy between the static dipoles of the i th and j th qubits can be written as $(1/4)U_{ij}^{(\text{st})}\sigma_z^i\sigma_z^j$, where $\sigma_z^i = |2\rangle_i\langle 2|_i - |1\rangle_i\langle 1|_i$ is the operator of the difference of the state occupations for the i th qubit, and

$$U_{ij}^{(\text{st})} = e^2 |z_{22} - z_{11}|^2 / d_{ij}^3. \quad (4)$$

The other dipole moment is associated with the $1 \rightarrow 2$ transition. If we use time-dependent wave functions, it oscillates in time at high frequency $\Omega_{12} = (E_2 - E_1)/\hbar$. Resonant

interaction between such oscillating dipoles has energy $(1/4)U_{ij}^{(\text{osc})}[\sigma_+^i\sigma_-^j + \text{H.c.}]$, where $\sigma_+^i = [\sigma_-^i]^\dagger = 2|2\rangle_i\langle 1|_i$ is the $1 \rightarrow 2$ transition operator for the i th qubit, and

$$U_{ij}^{(\text{osc})} = e^2 |z_{12}|^2 / d_{ij}^3. \quad (5)$$

The interaction between static and oscillating dipoles is non-resonant and can be safely neglected.

Interactions (4) and (5) allow implementation of a Controlled-NOT two-qubit gate and of interqubit excitation transfer, respectively.^{15,16} For a typical dipole moment er_B , the interaction energy $e^2 r_B^2 / d_{ij}^3$ between the qubits separated by $d_{ij} = 1 \mu\text{m}$ is 2×10^7 Hz, in frequency units. This energy is very sensitive to d_{ij} and can be increased by reducing the interelectron distance. Equations (4) and (5) apply for d_{ij} less than the distance from the electrons to the grounded plate in Fig. 1; for larger d_{ij} the interaction is screened and falls down as d_{ij}^{-5} . In practice it means that the interqubit coupling is likely to be limited to nearest and probably next-nearest neighbors.

The matrix elements z_{nm} depend on the overall field E_\perp that presses electrons against the helium surface. They can be obtained by solving a one-dimensional Schrödinger equation for the potential $-\Lambda z^{-1} + eE_\perp z$ with a hard wall at $z=0$ [cf. Eq. (2); we note that the total field E_\perp differs from the field \mathcal{E}_\perp produced by one electrode, see below]. The results are shown in Fig. 2.

The difference $z_{22} - z_{11}$ sharply decreases with increasing field for small E_\perp because of field-induced squeezing of the wave functions, which is particularly strong for the wave function of the excited state $|2\rangle$. The interplay between the squeezing and better overlapping of the wave functions $|1\rangle$ and $|2\rangle$ with increasing field leads to a weak field dependence of z_{12} for $eE_\perp r_B / R \lesssim 1$. It is seen from Fig. 2 and Eq. (4) that, for weak pressing field $E_\perp < 300$ V/cm, the energy of the “static” interaction is higher than its estimate given above by a factor varying from 20 to 4 with increasing E_\perp , because of the large numerical value of $(z_{22} - z_{11})/r_B$. It is also significantly higher than the energy given by Eq. (5).

A substantial part of single- and two-qubit operations is tuning targeted qubits in resonance with microwave radiation and with each other. It is accomplished by varying fields \mathcal{E}_\perp from the corresponding electrodes and thus Stark shifting the qubit transition frequencies $(E_2 - E_1)/\hbar$, cf. Fig. 2. In the simple case of one microwave frequency, the transition frequencies of different qubits will be tuned away from it and from each other by $\sim 1 - 10$ GHz, which determines the range over which they have to be varied. The transition frequency is changed by 1 GHz if \mathcal{E}_\perp is changed by ~ 1 V/cm. The respective change of the electrode potential is ~ 0.3 mV for $h = 0.5 \mu\text{m}$ and $r_{\text{el}} = 0.1 \mu\text{m}$. It can be accomplished over the time $\sim 10^{-8}$ s using standard means. Since the fields \mathcal{E}_\perp on different electrodes differ by ~ 1 V/cm or $\sim 1\%$, in Eqs. (4) and (5) we assumed that the matrix elements z_{nm} are the same for different qubits. Overall, for interelectron distances $d \lesssim 1 \mu\text{m}$, the qubit-qubit interaction limits the clock frequency of the quantum computer Ω_{QC} to $10^7 - 10^8$ Hz.

2. Limitations from many-electron effects

The electron energy spectrum should be formed so as to minimize the electron relaxation rate. One of the most “dangerous” relaxation processes is quasielastic scattering by capillary waves on helium surface, ripples, in which an electron makes a transition between its states and a ripplon is emitted or absorbed. This scattering is responsible for finite electron lifetime T_1 . Typical energies of appropriate ripples are extremely small, $\sim 10^{-3}$ K (see below). Therefore, the scattering can be eliminated for a one-qubit system, if none of the excited vibrational levels of the state $|1\rangle$ is in resonance with the ground vibrational level of the state $|2\rangle$ shown with a bold line in Fig. 2.

From Eq. (3), for a field $\mathcal{E}_\perp = 500$ V/cm and $h = 0.5\mu\text{m}$ we have $\omega_\parallel/2\pi \approx 2.1 \times 10^{10}$ Hz ≈ 1.0 K. Even though the spacing between vibrational levels is less than the energy gap $E_2 - E_1 \sim 6-10$ K, with so big ω_\parallel it is easy to avoid resonance between E_2 and an excited vibrational level of the state 1, i.e. between $E_2 - E_1$ and $n\hbar\omega_\parallel$.

The situation becomes more complicated for a system of interacting qubits. The interaction leads to coupling of in-plane vibrations of different electrons. In a many-electron system the vibrational energy spectrum becomes bandlike. One can think that each vibrational level in Fig. 2 becomes a bottom of a band of in-plane vibrational excitations. We will assume that the width of the lowest band Δ_\parallel is small compared to ω_\parallel . The width of the ν th band is then $\sim \nu\Delta_\parallel$ for not too large ν . To avoid quasielastic scattering by ripples, the vibrational bands should be well separated from each other up to energies $E_2 - E_1$, that is for $\nu \sim (E_2 - E_1)/\hbar\omega_\parallel$. This means that

$$\Delta_\parallel \ll \hbar\omega_\parallel^2/(E_2 - E_1). \quad (6)$$

The value of Δ_\parallel depends on the geometry of the many-electron system. It can be found if the electrodes and the electrons above them form a regular 2D array, or in other words, the electrons form a Wigner crystal with the same lattice constant as the electrodes. Then, if the phonon frequencies of the free-standing crystal in the absence of the electrode potential are $\omega_{\mathbf{k}j}$ (\mathbf{k} is the wave vector and $j = 1, 2$ is the branch number), then the vibrational frequencies of the pinned crystal are $(\omega_{\mathbf{k}j}^2 + \omega_\parallel^2)^{1/2}$. The phonon bandwidth is small compared to ω_\parallel provided $\omega_{\mathbf{k}j} \ll \omega_\parallel$, in which case $\Delta_\parallel = \max \omega_{\mathbf{k}j}^2/\omega_\parallel \sim \omega_p^2/\omega_\parallel$, where $\omega_p = (2\pi e^2 n_e^{3/2}/m)^{1/2}$ is the characteristic zone-boundary frequency of the free-standing Wigner crystal (n_e is the electron density).

It follows from the above arguments and condition (6) that quasielastic scattering will be eliminated for a pinned Wigner crystal, provided

$$\omega_p^2 \ll \hbar\omega_\parallel^3/(E_2 - E_1). \quad (7)$$

This imposes an upper limit on the nearest-neighbor spacing $d = \min d_{ij}$, because $\omega_p \propto d^{-3/2}$. For a square lattice with $d = 1\mu\text{m}$ we have $\omega_p/2\pi \approx 6.3$ GHz.

For the multielectrode system, the frequency ω_\parallel itself depends on the interelectrode distance d . If the electrode radius r_{el} is small compared to the depth h , the effect of the elec-

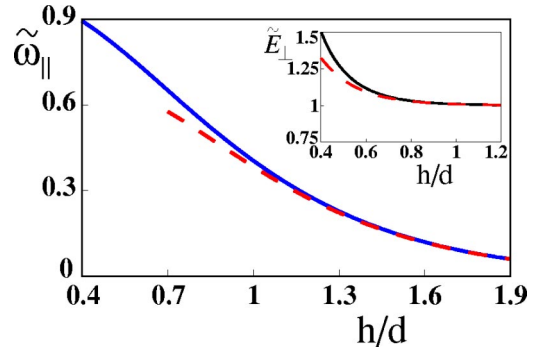


FIG. 3. (Color online) In-plane frequency $\tilde{\omega}_\parallel = \omega_\parallel/\omega'_\parallel$ and normal to the surface field $\tilde{E}_\perp = E_\perp/E'_\perp$ for an electron above a square array of electrodes. The electron is localized at height h above one of the electrodes. The interelectrode spacing is d . Electrodes are modeled by small spheres, $r_{\text{el}}/h \ll 1$, with same positive potential V_{el} . The scaling frequency $\omega'_\parallel = (eV_{\text{el}}r_{\text{el}}/mh^3)^{1/2}$ is given by Eq. (3) and corresponds to the limit $d \rightarrow \infty$. The scaling field is $\tilde{E}'_\perp = 2\pi n_e V_{\text{el}} r_{\text{el}}$. Asymptotic behavior of $\tilde{\omega}_\parallel$ and \tilde{E}_\perp for large $2\pi h/d$ is shown with dashed lines.

trostatic image in the electrode [in particular, the second term in Eq. (3) for \mathcal{E}_\perp] can be ignored. The overall potential of the electrode lattice at a distance z from helium surface ($z+h > 0$) is

$$V(\mathbf{r}, z) = 2\pi n_e V_{\text{el}} r_{\text{el}} \sum_{\mathbf{G}}' G^{-1} \exp(i\mathbf{G}\mathbf{r}) e^{-G(z+h)} - 2\pi n_e V_{\text{el}} r_{\text{el}} (z+h), \quad (8)$$

where \mathbf{G} is the reciprocal lattice vector.

The dependence of ω_\parallel on h/d for a square electrode array is shown in Fig. 3 along with the h/d dependence of the total normal field from the electrodes. The electrostatic in-plane confinement is due to the spatial nonuniformity of the electrode potential. Therefore ω_\parallel falls down as $2\pi(2eV_{\text{el}}r_{\text{el}}/md^3)^{1/2} \exp(-\pi h/d)$ for large $2\pi h/d$. However, as seen from Fig. 3, ω_\parallel remains close to the single-electrode value (3) for $h/d \leq 0.5$. This gives the desirable range of the aspect ratio h/d .

3. The overall pressing field E_\perp

The total perpendicular field on a localized electron E_\perp comes from the electrodes and the parallel-plate capacitor with the plates parallel to the helium surface. The lower plate is submerged into helium and is shown in Fig. 1. The upper plate is above the surface and further away; it is not shown. As we will see, the squeezing of the electron wave functions by the field E_\perp (cf. Fig. 2) increases the electron relaxation rate. Therefore, E_\perp should be minimized. At the same time, the electrostatic confinement (the frequency ω_\parallel) increases with the increasing field from the electrodes. It would be good to compensate the out-of-plane field E_\perp while keeping the in-plane potential as strongly confining as possible. This

can be accomplished by using a field from the capacitor, which is uniform in the plane and does not affect in-plane confinement.

The limitation on the compensating capacitor field comes from the condition that the overall field behind the electron layer should attract electrons to helium, otherwise they will leave the surface. This field is formed not only by the externally applied potentials, but also by the electron layer itself. The total averaged over \mathbf{r} applied field in the electron plane should therefore exceed $4\pi n_e$. In other words, the uniform component $2\pi n_e V_{\text{el}} r_{\text{el}}$ of the electrode field $-\partial_z V|_{z=0}$ (8) can be compensated down to $4\pi n_e$. The remaining pressing field on the electron E_{\perp} becomes then $C \times 2\pi n_e V_{\text{el}} r_{\text{el}} + 2\pi n_e$ with small C ($C \approx 0.24$ for $h/d = 0.5$, as seen from Fig. 3).

We note that the frequency ω_{\parallel} can be further increased electrostatically without increasing E_{\perp} by using a more sophisticated configuration of electrodes. Analysis of such configurations is outside the scope of this paper. We note also that, for sufficiently large ω_{\parallel} , the curvature of the electrode potential (8) in the z direction may become substantial, particularly for highly excited states of out-of-plane motion. However, for a typical $\omega_{\parallel}/2\pi = 20$ GHz, the effective curvature-induced change of the out-of-plane field for lowest states $2m\omega_{\parallel}^2 r_B/e$ is only ≈ 14 V/cm.

C. Electrostatic force on helium

Electric field from the electrodes and pressure from the electrons (polaronic effect) lead to deformation of the helium surface. The effect of the electrode potential can be easily estimated by noticing that the dielectric constant of helium is close to one, $\varepsilon - 1 \approx 0.057 \ll 1$. Therefore, if the surface is raised by $\xi(\mathbf{r})$, the associated change in the density (per unit area) of the free energy of helium $\Delta\mathcal{F}$ in the surface field $\mathbf{E}(\mathbf{r})$ is $-(\varepsilon - 1)E^2(\mathbf{r})\xi(\mathbf{r})/8\pi$. Bending of the surface is counteracted by surface energy, with density $\sigma(\partial\xi/\partial\mathbf{r})^2/2$, where σ is the surface tension. The competition between these two terms gives the height $\xi \sim (\varepsilon - 1)E_{\perp}^2 h^2/8\pi\sigma$ for $h \sim d$. For typical $E_{\perp} = 3 \times 10^2$ V/cm, $h = 0.5 \mu\text{m}$, and $d = 1 \mu\text{m}$ this gives a negligibly small $\xi < 10^{-10}$ cm. Therefore, this effect can be safely ignored.

III. DECAY OF THE EXCITED ELECTRON STATE

A. The Hamiltonian of coupling to surface displacement

The major mechanism of electron relaxation for low temperatures is scattering by vibrations of the liquid helium surface. A complete calculation of the energy of coupling to surface vibrations is nontrivial. The density profile of the interface between helium and its vapor has a complicated form, with the 10%/90% interfacial width $\approx 6-7$ Å, for low temperatures.²⁹ As a consequence, even for a flat surface the electron potential is more complicated than the simple image potential $-\Lambda/z$ for $z > 0$ and a sharp wall at $z = 0$ (2).²⁵ In particular the repulsive barrier is smooth, it becomes high compared to the binding energy R already on the tail of the helium density distribution. The spatial structure of surface excitations is complicated as well. However, for excitations

with sufficiently long wavelengths to a good approximation the vibrating helium surface can still be considered as a corrugated infinitely high potential wall. The electron wave function is set equal to zero on the surface.

In this approximation the Hamiltonian H_i of interaction of an electron with surface vibrations is obtained by changing the electron coordinates $\mathbf{r} \rightarrow \mathbf{r}$, $z \rightarrow z - \xi(\mathbf{r})$ where $\xi(\mathbf{r})$ is the surface displacement, see Refs. 30–32. The interaction is a series in the ratio ξ/r_B . Typically this ratio is very small, $\sim 3 \times 10^{-3}$ for thermal displacement with characteristic wave numbers. Therefore, to a good approximation H_i can be expanded in ξ , keeping only lowest-order terms. The major term, $H_i^{(1)}$, is linear in $\xi(\mathbf{r}) = \sum_{\mathbf{q}} \xi_{\mathbf{q}} e^{i\mathbf{q}\mathbf{r}}$,

$$H_i^{(1)} = \sum_{\mathbf{q}} \xi_{\mathbf{q}} e^{i\mathbf{q}\mathbf{r}} \hat{V}_{\mathbf{q}}, \quad (9)$$

with

$$\hat{V}_{\mathbf{q}} = -\frac{i}{m}(\mathbf{q} \cdot \hat{\mathbf{p}}) \hat{p}_z - \frac{i\hbar}{2m} q^2 \hat{p}_z + eE_{\perp} + \Lambda q^2 v_{\text{pol}}(qz),$$

$$v_{\text{pol}}(x) = x^{-2} [1 - xK_1(x)]. \quad (10)$$

Here, $\hat{\mathbf{p}} = -i\hbar\partial_{\mathbf{r}}$ is the 2D electron momentum, and $\hat{p}_z = -i\hbar\partial_z$. The first two terms in the operator $\hat{V}_{\mathbf{q}}$ describe a *kinematic* interaction, which arises because the electron wave function is set equal to zero on a nonflat surface. The term $v_{\text{pol}}(qz)$ describes the change of the polarization energy due to surface curvature^{31,32} [$K_1(x)$ is the modified Bessel function].

The quadratic in ξ coupling is

$$H_i^{(2)} = \sum_{\mathbf{q}_1, \mathbf{q}_2} \xi_{\mathbf{q}_1} \xi_{\mathbf{q}_2} \exp[i(\mathbf{q}_1 + \mathbf{q}_2)\mathbf{r}] \hat{V}_{\mathbf{q}_1 \mathbf{q}_2}. \quad (11)$$

As in the case of linear coupling, it also has a kinematic part discussed in Ref. 32 and a polarization part,

$$\hat{V}_{\mathbf{q}_1 \mathbf{q}_2} = \hat{V}_{\mathbf{q}_1 \mathbf{q}_2}^{(k)} + \hat{V}_{\mathbf{q}_1 \mathbf{q}_2}^{(\text{pol})}, \quad \hat{V}_{\mathbf{q}_1 \mathbf{q}_2}^{(k)} = -(\mathbf{q}_1 \mathbf{q}_2) p_z^2 / 2m. \quad (12)$$

The polarization coupling parameters can be obtained in the same way as it was done^{31,32} for the linear coupling constants $\propto v_{\text{pol}}(qz)$. They have the form

$$\hat{V}_{\mathbf{q}_1 \mathbf{q}_2}^{(\text{pol})} = -\Lambda z^{-3} [1 - u(q_1 z) - u(q_2 z) + u(|\mathbf{q}_1 + \mathbf{q}_2| z)],$$

$$u(x) = x^2 K_2(x) / 2 \quad (13)$$

1. Coupling to ripples

The biggest contribution to surface vibrations comes from capillary waves, ripples. The corresponding displacement $\xi_{\mathbf{q}}$ is related to the creation and annihilation operators of ripples by

$$\xi_{\mathbf{q}} = S^{-1/2} (\hbar q / 2\rho\omega_q)^{1/2} (b_{\mathbf{q}} + b_{-\mathbf{q}}^{\dagger}), \quad (14)$$

where S is the area of the system, ρ is the helium density, and the ripplon frequency $\omega_q = (\sigma q^3 / \rho)^{1/2}$ for $q \gg (\rho g / \sigma)^{1/2}$.

The change of variables used to take into account the hard wall potential on helium surface leads also to extra terms in

the kinetic energy of riplons coupled to the electron, which is yet another source of electron-riplon coupling.³² Compared to similar terms in Eqs. (9) and (11), these terms have an extra parameter $\omega_q m / \hbar q^2$, which is extremely small for typical q .

There are several limitations on the wave numbers q of riplons for which the electron-riplon coupling has the form (9)–(13). Monarkha and Shikin³² argue that essentially qr_B should be $\lesssim 1$. This could be too restrictive. But we believe that q should certainly be small compared to the reciprocal width of the helium liquid-vapor interface and the reciprocal decay length of the electron wave function into helium (note that there is no factor 2π here, because a capillary wave with wave number \mathbf{q} decays into helium as $\exp(qz)$, for a sharp interface). Both lengths are of order of a few angstroms, which means that the large- q cutoff q_{\max} should be $\lesssim 10^7 \text{ cm}^{-1}$.

A cutoff at 10^7 cm^{-1} is consistent also with the condition that $H_i^{(2)}$ (11) should be small. The effect of $H_i^{(2)}$ is seen already in the first order of the perturbation theory. It comes primarily from large- q terms in the kinematic part in Eq. (12). For the relevant wave numbers $\hbar\omega_q \gg k_B T$, and therefore from Eq. (14) we have $\langle \xi_{\mathbf{q}_1} \xi_{\mathbf{q}_2} \rangle \approx S^{-1} \delta_{\mathbf{q}_1, -\mathbf{q}_2} \hbar q_1^{-1/2} / 2(\sigma\rho)^{1/2}$. This gives the relative change of the electron kinetic energy for motion transverse to the surface

$$\delta K / K = \hbar q_{\max}^{7/2} / 14\pi(\sigma\rho)^{1/2}.$$

Clearly, δK very strongly depends on the cutoff wave number q_{\max} . Numerical estimates give $\delta K / K \approx 3 \times 10^{-4}$ for $q_{\max} = 10^7 \text{ cm}^{-1}$, whereas for $q_{\max} = 10^8 \text{ cm}^{-1}$ the relative change of the kinetic energy would be equal to one. Finding H_i for $q \gg 10^7 \text{ cm}^{-1}$ requires a full calculation of the ripplon-induced modulation of the electron potential for the diffuse helium surface, which is not a subject of the present paper.

In what follows we will use spectroscopic notations and define the decay rate Γ as the rate of decay of the off-diagonal matrix element ρ_{12} of the electron density matrix. So defined, Γ gives the decay-induced contribution to the half-width of the peak in the spectrum of microwave absorption. It is related to the lifetime T_1 of the electron excited state by $\Gamma = (2T_1)^{-1}$.

B. One-riplon decay

An important consequence of strong in-plane electron confinement is that it essentially eliminates decay processes, in which an electron transition is accompanied by emission or absorption of one ripplon. This happens because riplons are very slow. Energy conservation in a transition requires too large ripplon momentum for an electron to accommodate.

Decay of the excited qubit state $|2,0,0\rangle$ does not require a transition into the ground state $|1,0,0\rangle$. An electron can emit a ripplon and make a transition $|2,0,0\rangle \rightarrow |1,\nu,m_\nu\rangle$ into any excited state $|1,\nu,m_\nu\rangle$ of in-plane vibrations in the state $|1\rangle$ of z motion, see Fig. 2. In the case of decay into low-frequency excitations, most “dangerous” are transitions with a minimal

electron energy change. These are transitions to the vibrational energy level of the state $|1\rangle$ with the energy closest to E_2 . It has the quantum number

$$\nu = \nu_c \equiv \text{int} [(E_2 - E_1) / \hbar\omega_{\parallel}]$$

($\text{int}[x]$ is the integer part of x). In the general case the electron energy change in a transition $|2,0,0\rangle \rightarrow |1,\nu_c,m_{\nu_c}\rangle$ is $\lesssim \hbar\omega_{\parallel}$.

The one-riplon decay rate is determined by the matrix elements $\langle 2,0,0 | \exp(i\mathbf{q}\mathbf{r}) \hat{V}_{\mathbf{q}} | 1,\nu_c,m_{\nu_c} \rangle$ of the electron-riplon coupling (9) and (10). They contain factors $\langle 0,0 | \exp(i\mathbf{q}\mathbf{r}) | \nu_c,m_{\nu_c} \rangle$. It is easy to see that these factors are exponentially small for $q \gg \nu_c^{1/2} / a_{\parallel}$, where

$$a_{\parallel} = (\hbar / m\omega_{\parallel})^{1/2} \quad (15)$$

is the electron in-plane localization length. The condition $q \lesssim \nu_c^{1/2} / a_{\parallel}$ determines the limiting wave number of riplons that may be emitted in an electron transition.

The frequency of riplons with $q = \nu_c^{1/2} / a_{\parallel}$ is much less than ω_{\parallel} , provided

$$\omega_{\parallel} \gg (\sigma/\rho)^{1/2} [m(E_2 - E_1) / \hbar^2]^{3/4}.$$

This inequality is satisfied already for $\omega_{\parallel} / 2\pi \gtrsim 0.2 \text{ GHz}$, whereas a typical ω_{\parallel} for confined electrons is $\sim 20 \text{ GHz}$. Therefore one-riplon decay is exponentially improbable. This result does not change for a many-electron system provided the bands of in-plane vibrations are narrow, as discussed in Sec. II B, see Eq. (6).

C. Two-riplon decay

Even for a large separation between electron energy levels, where one-riplon decay processes are exponentially suppressed, decay with emission of two riplons may still be possible.^{33,34} Indeed, each of the wave vectors $\mathbf{q}_1, \mathbf{q}_2$ of the emitted riplons can be large: it is only their sum that is limited by the reciprocal electron localization length. This means that $\mathbf{q}_1 \approx -\mathbf{q}_2$, i.e. the riplons propagate in opposite directions and have nearly same frequencies. They are determined by energy conservation, $\omega_{q_1} \approx \omega_{q_2} \approx \delta E / 2\hbar$, where δE is the electron energy change.

A characteristic minimal value of δE in an electron transition $|2,0,0\rangle \rightarrow |1,\nu,m_\nu\rangle$ is $\sim \hbar\omega_{\parallel}$. For a typical $\omega_{\parallel} / 2\pi = 20 \text{ GHz}$, the ripplon frequency ω_q becomes equal to $\omega_{\parallel} / 2$ when $q = 1.2 \times 10^7 \text{ cm}^{-1}$. For wave numbers that are so large, the theory (9)–(13) already overestimates the strength of the electron-riplon coupling. Even larger q are required for ripplon-induced transitions over several vibrational levels, because in such transitions the electron energy change exceeds $\hbar\omega_{\parallel}$. We will disregard them and discuss only minimal-energy transitions $|2,0,0\rangle \rightarrow |1,\nu,m_\nu\rangle$ with $\nu = \nu_c$. For these transitions

$$\delta E = E_2 - E_1 - \nu_c \hbar\omega_{\parallel}.$$

For typical temperatures of 10 mK we have $\hbar\omega_{q_{1,2}} \approx \delta E/2 \gg k_B T$, and electron decay occurs via spontaneous emission of riplons.

To find the two-riplon decay rate Γ_{2r} one should first calculate the matrix elements of the two-riplon coupling $H_i^{(2)}$ (11) on the relevant electron wave functions. They factor into products of matrix elements of out-of-plane and in-plane electron operators,

$$\begin{aligned} & \langle 2,0,0 | \hat{V}_{\mathbf{q}_1\mathbf{q}_2} \exp[i(\mathbf{q}_1 + \mathbf{q}_2)\mathbf{r}] | 1, \nu, m_\nu \rangle \\ &= \langle 2 | \hat{V}_{\mathbf{q}_1\mathbf{q}_2} | 1 \rangle \langle 0,0 | \exp[i(\mathbf{q}_1 + \mathbf{q}_2)\mathbf{r}] | \nu, m_\nu \rangle. \end{aligned} \quad (16)$$

The squared absolute values of the terms (16) should then be summed over the final states ν, m_ν and over $\mathbf{q}_{1,2}$. The summands have to be multiplied by an extra $\mathbf{q}_{1,2}$ -dependent weighting factor, which comes from the Fourier components of the ripplon-induced displacement of the helium surface $\xi_{\mathbf{q}_1}, \xi_{\mathbf{q}_2}$ (14) and from the energy conservation law.

The calculation is significantly simplified by the fact that the sum over m_ν can be found independently. This is because all states of in-plane electron vibrations $|\nu, m_\nu\rangle$ with same ν but different m_ν have same energies. We will use the relation

$$\begin{aligned} g(\nu, q) &= \sum_{m_\nu} |\langle 0,0 | e^{i\mathbf{q}\mathbf{r}} | \nu, m_\nu \rangle|^2 = x^\nu e^{-x} / \nu!, \\ x &= q^2 a_{\parallel}^2 / 2, \end{aligned} \quad (17)$$

where the electron localization length a_{\parallel} is given by Eq. (15). The function $g(\nu, q)$ (17) is exponentially small if $q \gg \nu^{1/2}/a_{\parallel}$.

For $\nu = \nu_c$, the sum over m_ν of the squared absolute values of the matrix elements (16) gives a factor $g(\nu_c, |\mathbf{q}_1 + \mathbf{q}_2|)$. This factor imposes the expected constraint on the typical ripplon wave vectors, $|\mathbf{q}_1 + \mathbf{q}_2| \lesssim \nu_c^{1/2}/a_{\parallel} \ll q_{1,2}$. In turn, this inequality significantly simplifies integration over $\mathbf{q}_1, \mathbf{q}_2$. One can set $\mathbf{q}_1 \approx -\mathbf{q}_2$ everywhere except for the function $g(\nu, |\mathbf{q}_1 + \mathbf{q}_2|)$, which can be easily integrated over $\mathbf{q}_1 + \mathbf{q}_2$.

We will analyze the contributions to the decay rate from the kinematic and polarization two-riplon couplings separately. The kinematic coupling is determined by the term $\hat{V}_{\mathbf{q}_1\mathbf{q}_2}^{(k)}$ (12) in $\hat{V}_{\mathbf{q}_1\mathbf{q}_2}$. Keeping only this term, we obtain the decay rate $\Gamma_{2r}^{(k)}$ as

$$\Gamma_{2r}^{(k)} = \frac{K_{12}^2 R^2 q_{\text{res}}^{7/2}}{24\pi a_{\parallel}^2 \rho^{1/2} \sigma^{3/2}}, \quad K_{12} = \frac{\langle 1 | p_z^2 / 2m | 2 \rangle}{R}. \quad (18)$$

Here, q_{res} is given by the condition $\omega_{q_{\text{res}}} = \delta E/2\hbar$. The decay rate is determined by the scaled matrix element of the kinetic energy of out-of-plane motion K_{12} . It is shown in Fig. 4.

The rate $\Gamma_{2r}^{(k)}$ depends on q_{res} and therefore on δE very steeply, $\Gamma_{2r}^{(k)} \propto \delta E^{7/3}$. For $\delta E = \hbar\omega_{\parallel}/4$ and $\omega_{\parallel}/2\pi = 20$ GHz we have $q_{\text{res}} \approx 4.6 \times 10^6 \text{ cm}^{-1}$ and $\Gamma_{2r}^{(k)} = 7.6 \times 10^2 - 3.8 \times 10^3 \text{ s}^{-1}$ for the pressing field $E_{\perp} = 0 - 300 \text{ V/cm}$. This

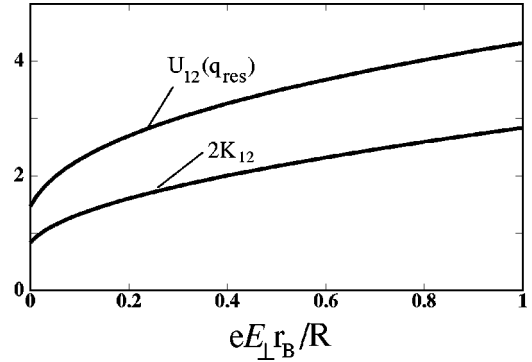


FIG. 4. The absolute values of the scaling factors K_{12} (18) and $U_{12}(q)$ (19) in the probabilities of scattering into two riplons due to the kinematic and polarization couplings, respectively. The riplons propagate in opposite directions with nearly same wave numbers q_{res} given by the energy conservation condition: $\omega_q = \delta E/2\hbar$ for $q = q_{\text{res}}$. Only transitions with smallest energy transfer δE are taken into account and the approximation of an infinite sharp potential wall for an electron at the helium surface is used. The data for U_{12} refer to $q_{\text{res}} = 3.5/r_B$, which corresponds to $\delta E/2\pi\hbar \approx 5 \text{ GHz}$.

value can be decreased by reducing δE . However, Eq. (18) is probably an overestimate even for the δE used above, because it is based on the approximation of an infinite-wall potential for an electron and the assumption that the helium surface is sharp.

The expression for the two-riplon decay rate $\Gamma_{2r}^{(\text{pol})}$ due to the polarization two-riplon interaction (13) has the same form as Eq. (18). Just the factor $K_{12}^2 q_{\text{res}}^{7/2}$ in Eq. (18) has to be replaced with $U_{12}^2(q_{\text{res}})/r_B^4 q_{\text{res}}^{1/2}$, where U_{12} is determined by the matrix element of $-2r_B^3 \hat{V}_{\mathbf{q}_1\mathbf{q}_2}^{(\text{pol})}/\Lambda$ (13) on the functions $|1\rangle, |2\rangle$. For typical $|\mathbf{q}_1 + \mathbf{q}_2| \lesssim \nu_c^{1/2}/a_{\parallel}$, the major contribution to this matrix element comes from the range of comparatively small $|\mathbf{q}_1 + \mathbf{q}_2|z$. Therefore, a good estimate can be obtained by replacing $K_2(|\mathbf{q}_1 + \mathbf{q}_2|z)$ with its small- z limit in Eq. (13) and by setting $q_1 = q_2 = q_{\text{res}}$ in the other terms in $\hat{V}_{\mathbf{q}_1\mathbf{q}_2}^{(\text{pol})}$. Then

$$U_{12}(q) = 2r_B^3 \langle 1 | z^{-3} [2 - q^2 z^2 K_2(qz)] | 2 \rangle. \quad (19)$$

The coefficient U_{12} as given by Eq. (19) is shown in Fig. 4. For δE and ω_{\parallel} chosen above we have $\Gamma_{2r}^{(\text{pol})}/\Gamma_{2r}^{(k)} \sim 0.1$ for $E_{\perp} = 0 - 300 \text{ V/cm}$. The rate $\Gamma_{2r}^{(\text{pol})}$ grows much slower than $\Gamma_{2r}^{(k)}$ with increasing q_{res} (and thus with increasing δE).

Besides the terms $\Gamma_{2r}^{(k)}$ and $\Gamma_{2r}^{(\text{pol})}$ due to purely kinematic and polarization mechanisms, there is a contribution to the decay rate from the interference of these two mechanisms. It is smaller than $\Gamma_{2r}^{(k)} + \Gamma_{2r}^{(\text{pol})}$ and will not be discussed.

D. Phonon-induced decay

An important channel of electron energy relaxation is decay into phonons in helium. For a typical energy transfer $\delta E \sim \hbar\omega_{\parallel}$, the wave numbers of the phonons participating in decay are $\sim \omega_{\parallel}/v_s$, where v_s is the sound velocity in helium.

They are much larger than the reciprocal in-plane localization length of the electron a_{\parallel}^{-1} , which limits the in-plane momentum transfer from electrons to phonons. As a result, only phonons propagating nearly normal to the surface (in the z direction) may be excited in a one-phonon decay (cf. Ref. 33).

1. Decay due to phonon-induced surface displacement

We propose two mechanisms of electron-phonon coupling that lead to qubit decay. One is related to phonon-induced displacement of the helium surface. This mechanism can be quantitatively described in the approximation of a sharp helium boundary, which provides an infinitely high potential barrier for electrons. The coupling is given by Eqs. (9) and (10) with $\xi_{\mathbf{q}}$ being now a phonon-induced component of the surface displacement. As in the case of coupling to ripples, it would be unreasonable to use this approximation for short-wavelength phonons, in particular for phonons with $Q_z \gg 10^7 \text{ cm}^{-1}$ (Q_z is the normal to the surface component of the electron-phonon wave vector). For typical $\omega_{\parallel}/2\pi = 20 \text{ GHz}$ we have $Q_z \sim \omega_{\parallel}/v_s \sim 5 \times 10^6 \text{ cm}^{-1}$. Therefore, we will again consider decay of the state $|2,0,0\rangle$ into closest lower-energy states $|1, \nu_c, m_{\nu_c}\rangle$.

For a typical $\mathbf{q} \equiv (q_x, q_y) \sim 1/a_{\parallel}$ and $Q_z \lesssim \omega_{\parallel}/v_s$ we have $\sigma q^2/\rho v_s^2 Q_z \ll 1$. This inequality allows one to think of the helium surface as a free boundary for phonons and to ignore coupling between phonons and ripples.^{35,36} Then surface displacement is simply related to the Fourier components $u_{\mathbf{Q}}$ of the phonon displacement field [here, $\mathbf{Q} = (\mathbf{q}, Q_z)$ is the 3D phonon wave vector, and $u_{\mathbf{Q}}$ is the displacement along \mathbf{Q}]. In turn, $u_{\mathbf{Q}}$ is related to the operators of creation and annihilation of phonons in a standard way,

$$u_{\mathbf{Q}} = (\hbar/2\rho V v_s Q)^{1/2} (c_{\mathbf{Q}} - c_{-\mathbf{Q}}^{\dagger}) \quad (20)$$

(V is the volume of helium).

From Eqs. (9), (10), and (20), we obtain the rate of decay $|2,0,0\rangle \rightarrow |1, \nu_c, m_{\nu_c}\rangle$ due to phonon-induced surface displacement in the form

$$\Gamma_{\text{ph}}^{(s)} = (8\pi^2 \rho v_s \delta E)^{-1} \sum_{m_{\nu_c}=0}^{\nu_c} \int d\mathbf{q} |\langle 2,0,0 | e^{i\mathbf{q}\mathbf{r}} \hat{V}_{\mathbf{q}} | 1, \nu_c, m_{\nu_c} \rangle|^2. \quad (21)$$

Here, we have used that $Q_z \gg q \equiv (q_x^2 + q_y^2)^{1/2}$. Integration over Q_z is done by replacing the phonon wave number Q with Q_z in the energy conservation law $\delta(\hbar v_s Q - \delta E)$. We also replaced Q with Q_z in the expansion coefficients Eq. (20) of the phonon displacement field.

We start with the contribution to $\Gamma_{\text{ph}}^{(s)}$ from the kinematic terms in $\hat{V}_{\mathbf{q}}$ [the first two terms in Eq. (10)]. The matrix element of the sum of these terms [weighted with $\exp(i\mathbf{q}\mathbf{r})$] on the wave functions of in-plane electron vibrations is

$$\begin{aligned} & \langle 0,0 | \exp(i\mathbf{q}\mathbf{r}) [(\hat{\mathbf{q}}\mathbf{p}) + \hbar q^2/2] | \nu, m_{\nu} \rangle \\ & = -\nu m \omega_{\parallel} \langle 0,0 | \exp(i\mathbf{q}\mathbf{r}) | \nu, m_{\nu} \rangle. \end{aligned}$$

The sum over m_{ν} in Eq. (21) can be then calculated using Eq. (17). This gives the following expression for the kinematic contribution to the decay rate,

$$\Gamma_{\text{ph}}^{(s;k)} \approx (E_2 - E_1)^2 z_{12}^2 \frac{\nu_c^2 m^3 \omega_{\parallel}^3}{4\pi\rho v_s \hbar^3 \delta E}. \quad (22)$$

The numerical value of $\Gamma_{\text{ph}}^{(s;k)}$ is $7.8 \times 10^2 \text{ s}^{-1}$ for $E_{\perp} = 0$, $\omega_{\parallel}/2\pi = 21.1 \text{ GHz}$, and $\delta E \approx \hbar \omega_{\parallel}$ ($\nu_c = 5$ in this case). It goes up to $\sim 1.5 \times 10^4 \text{ s}^{-1}$ for $E_{\perp} = 300 \text{ V/cm}$ and $\omega_{\parallel}/2\pi = 20.6 \text{ GHz}$ (in this case $\nu_c = 12$). The values of ω_{\parallel} were adjusted here to meet the condition $\delta E = E_2 - E_1 - \nu_c \hbar \omega_{\parallel} \approx \hbar \omega_{\parallel}$ for the energy spectrum calculated for a sharp helium boundary; the real level spacing is a few percent smaller,²⁴⁻²⁷ leading to a slightly smaller $\Gamma_{\text{ph}}^{(s;k)}$ for $\omega_{\parallel}/2\pi \sim 20 \text{ GHz}$. We expect a more significant change (reduction) of $\Gamma_{\text{ph}}^{(s;k)}$ due to diffuseness of helium surface.

The contribution to $\Gamma_{\text{ph}}^{(s)}$ from the polarization term in $\hat{V}_{\mathbf{q}}$ [the last term in Eq. (10)] can be calculated similarly and has the form

$$\Gamma_{\text{ph}}^{(s; \text{pol})} \approx \frac{4R^2 r_B^2}{\nu_c! \pi \rho v_s \delta E a_{\parallel}^6} \int_0^{\infty} dx e^{-x} x^{\nu_c+2} v^2(x), \quad (23)$$

where $v^2(x) = |\langle 1 | v_{\text{pol}}[(2x)^{1/2} z/a_{\parallel}] | 2 \rangle|^2$. The numerical value of $\Gamma_{\text{ph}}^{(s; \text{pol})}$ is $\sim 7 \times 10^2 \text{ s}^{-1}$ for $E_{\perp} = 0$ and goes up to $\sim 7 \times 10^3 \text{ s}^{-1}$ for $E_{\perp} = 300 \text{ V/cm}$ (we used same ω_{\parallel} as in the above estimate of $\Gamma_{\text{ph}}^{(s;k)}$).

There exists also a contribution to $\Gamma_{\text{ph}}^{(s)}$ (21) from the interference of the polarization and kinematic interactions discussed above. It is bilinear in the corresponding terms in $\hat{V}_{\mathbf{q}}$ Eq. (10) and can be obtained from (21) in the same way as the decay rates $\Gamma_{\text{ph}}^{(s;k)}$, $\Gamma_{\text{ph}}^{(s; \text{pol})}$ (22) and (23). The resulting expression is of the same order of magnitude as Eqs. (22) and (23).

The scattering rate $\Gamma_{\text{ph}}^{(s)}$ can be reduced by decreasing the pressing field E_{\perp} . It can also be reduced by going to a higher confinement frequency ω_{\parallel} . With increasing ω_{\parallel} the wavelength of the phonons participating in electron decay will decrease and ultimately become smaller than the width of the diffuse layer on helium surface (in fact, the above calculation probably already overestimates the scattering rate). In this case scattering by phonons will be largely suppressed. The frequency ω_{\parallel} can be increased by using a more complicated electrode configuration. The spectrum of in-plane electron excitations can be also controlled by a magnetic field applied transverse to the helium surface, as initially suggested for qubits in Ref. 15.

2. Decay due to phonon-induced modulation of the helium dielectric constant

Another mechanism of coupling to phonons is through phonon-induced modulation of the image potential of an electron. It results from the modulation of the helium density $\delta\rho$ and related modulation of the dielectric constant $\delta\epsilon$. It is

reasonable to assume that, for long-wavelength phonons, $\delta\varepsilon = (\varepsilon - 1)\delta\rho/\rho$. To lowest order in $\varepsilon - 1$, $\delta\varepsilon$ the coupling energy is

$$H_i^{(d)} = -\frac{1}{8\pi} \int d\mathbf{R}' \delta\varepsilon(\mathbf{R}') E^2(\mathbf{R}'; \mathbf{R}). \quad (24)$$

Here the integration goes over the space occupied by helium, $\mathbf{R} \equiv (\mathbf{r}, z)$ is the 3D position vector, and $\mathbf{E}(\mathbf{R}'; \mathbf{R})$ is the electric field at \mathbf{R}' created by an electron located at a point \mathbf{R} . This field is calculated for free space. Equation (24) is obtained in a standard way from the electrostatic energy of a dielectric with a dielectric constant close to one in an external field $\mathbf{E}(\mathbf{R}'; \mathbf{R})$.

Using Eq. (24), the coupling Hamiltonian can be then written in the form

$$H_i^{(d)} = \sum_{\mathbf{Q}} u_{\mathbf{Q}} \exp(i\mathbf{q}\mathbf{r}) \hat{V}_{\mathbf{Q}}^{(d)}, \quad \hat{V}_{\mathbf{Q}}^{(d)} = i\Lambda q Q v^{(d)} \quad (25)$$

with $v^{(d)} \equiv v^{(d)}(q, Q_z, z)$ being

$$v^{(d)} = \int_0^\infty dz' (z+z')^{-1} e^{-iQ_z z'} K_1[q(z+z')]. \quad (26)$$

As in the case discussed in the preceding section, coupling (25) gives rise to transitions between electron energy levels accompanied by emission of phonons. Here, too, the typical in-plane wave numbers of emitted phonons q are much less than the normal to the surface wave number $Q_z \approx \delta E/\hbar v_s$. The expression for the corresponding decay rate $\Gamma_{\text{ph}}^{(d)}$ has the form

$$\Gamma_{\text{ph}}^{(d)} \approx \frac{R^2 \delta E r_B^2}{\pi \hbar^2 \rho v_s^3} \int_0^\infty dq q^3 |\langle 2|v^{(d)}|1\rangle|^2 g(v_c, q). \quad (27)$$

Evaluation of the integral is largely simplified by the fact that the function $q^3 g(v, q)$ sharply peaks at $q = q_v \approx (2v + 3)^{1/2}/a_{\parallel}$. Therefore, with an error less than 10% one can replace $v^{(d)}$ in Eq. (27) by its value (26) for $q = q_v$.

For $\omega_{\parallel}/2\pi = 20$ GHz and $\delta E = \hbar\omega_{\parallel}$, the value of $\Gamma_{\text{ph}}^{(d)}$ varies from $\sim 1 \times 10^4 \text{ s}^{-1}$ to $\sim 6 \times 10^4 \text{ s}^{-1}$ with E_{\perp} increasing from 0 to 300 V/cm. However, these values have to be taken with care. The integrand in $v^{(d)}$ (26) is a fast oscillating function of z' on the characteristic scale $z' \sim r_B$, because typically $Q_z r_B \gg 1$ ($Q_z r_B \approx 4$ for chosen ω_{\parallel}). In addition, the integrand of the matrix element of $v^{(d)}$ in Eq. (27) has an integrable singularity for $z = z' = 0$ [the wave functions $\psi_n(z) \propto z$ for $z \rightarrow 0$]. As a result, a significant contribution to the matrix element comes from small distances from the helium surface, $z' \ll r_B$. Changing, in view of diffuseness of helium surface, the limit of integration in Eq. (26) from $z' = 0$ to a more reasonable $z' = r_B/10$ reduces the value of $\Gamma_{\text{ph}}^{(d)}$ by a factor of 3.

The decay rate $\Gamma_{\text{ph}}^{(d)}$ decreases with the increasing δE roughly as $1/\delta E$ (and even faster, in view of the ‘‘dead’’ layer on the diffuse surface). For higher δE and, respectively, for higher wave numbers of resonant phonons, the simple approximation (25) no longer describes the electron-

phonon interaction. Therefore, as in the case of scattering due to phonon-induced surface deformation, a way to reduce the scattering rate is to increase the frequency of in-plane vibrations.

Full coupling to phonons is given by the sum of the kinematic and polarization couplings parameters $\hat{V}_{\mathbf{q}}$ and $\hat{V}_{\mathbf{Q}}^{(d)}$. Therefore, the total rate of phonon scattering contains cross terms which describe interference of the coupling mechanisms. These terms do not change the overall estimate of the rate.

We note that an interesting situation may occur if one of the transition frequencies of the electron comes in resonance with the roton energy. In this case we expect an increase of the decay rate. Observing it would be a direct demonstration of coupling to volume excitations in helium.

E. Radiative decay

Even though the dipole matrix element for the electron transition $2 \rightarrow 1$ is large, the rate of radiative decay $\sim e^2 z_{12}^2 R^3/\hbar^4 c^3 \approx 2 \text{ s}^{-1}$ is extremely small. For low- \mathbf{Q} microwave cavities or waveguides which will be used in experiment, radiative decay will play no role in electron relaxation.

IV. DEPHASING DUE TO RIPPLON SCATTERING

In addition to depopulation of the excited state of a qubit, electron coupling to excitations in liquid helium leads also to dephasing, i.e. diffusion of the phase difference between the qubit states $|2,0,0\rangle$ and $|1,0,0\rangle$. The dephasing results from random modulation, by thermal fluctuations in helium, of the distance between the energy levels 1 and 2. In other terms it can be described as quasielastic scattering of thermal excitations off an electron. The scattering is different in different electron states. Therefore, it randomizes the phase difference between the wave functions of the states without causing interstate transitions. The corresponding decoherence mechanism is known for defects in solids³⁷ as modulational or Raman broadening. For electrons on helium it was discussed in Refs. 15 and 33.

Dephasing comes primarily from coupling to ripples, because they are soft. The density of states of thermally excited ripples is comparatively high even for low temperatures. At the same time, thermal occupation numbers of the ripples coupled to an electron by one-ripple coupling $H_i^{(1)}$ are large. Indeed, the typical wave number q_r and frequency ω_r of such ripples are

$$q_r = 1/a_{\parallel}, \quad \omega_r \equiv \omega_{q_r} = (\sigma/\rho)^{1/2} q_r^{3/2}. \quad (28)$$

For $\omega_{\parallel}/2\pi = 20$ GHz we have $\omega_r/2\pi \approx 4.8 \times 10^7 \text{ Hz} \approx 2.3 \text{ mK}$, i.e. $\hbar\omega_r \ll k_B T$ even for temperatures as low as 10 mK. As we will see, the dephasing rate depends on the both typical ripplon frequencies, ω_r and $k_B T/\hbar$.

For completeness, we will briefly outline a simple way to obtain the dephasing rate due to an electron-ripple coupling H_i (a more consistent approach is based on the master equation, but it gives the same result). To first order in H_i , the

changes of the electron energies $\delta\hat{E}_{1,2}$ of the states $|1,0,0\rangle, |2,0,0\rangle$ are determined by the diagonal matrix elements of H_i on the corresponding wave functions. These matrix elements are operators with respect to riplons. In the interaction representation the ripplon coordinates $\xi_{\mathbf{q}}$ become functions of time. The typical ripplon frequencies $\omega_r, k_B T/\hbar$ are small compared to the electron transition frequencies $\sim \omega_{\parallel}$. Therefore, in the spirit of the adiabatic approximation, the electron energies $\delta\hat{E}_{1,2}$ become parametrically dependent on time in terms of $\xi_{\mathbf{q}}(t)$. So does also the change in the interlevel distance

$$\delta\hat{E}_{21}(t) = \langle 2,0,0 | H_i(t) | 2,0,0 \rangle - \langle 1,0,0 | H_i(t) | 1,0,0 \rangle. \quad (29)$$

The average value of the energy difference (29), $\langle \delta\hat{E}_{21}(t) \rangle$, is independent of time (here and below $\langle \cdot \rangle$ means averaging over the thermal distribution of riplons). It gives a shift of the transition frequency of the qubit. In what follows we will assume that this shift has already been incorporated into $E_{1,2}$ and set $\langle \delta\hat{E}_{21}(t) \rangle = 0$.

The increment of the phase difference $\delta\hat{\phi}_{21}(t)$ between the states 1,2 is given by the integral of $\delta\hat{E}_{21}$ over time. From Eq. (29) we have for the mean-square phase increment

$$\begin{aligned} \delta\varphi_{21}^2(t) &\equiv \langle [\delta\hat{\phi}_{21}(t) - \delta\hat{\phi}_{21}(0)]^2 \rangle \\ &= \hbar^{-2} \int \int_0^t dt_1 dt_2 \langle \delta\hat{E}_{21}(t_1) \delta\hat{E}_{21}(t_2) \rangle. \end{aligned} \quad (30)$$

The operator $\delta\hat{E}_{21}(t)$ has two typical frequencies, ω_r and $k_B T/\hbar$. Therefore, the correlator $\langle \delta\hat{E}_{21}(t_1) \delta\hat{E}_{21}(t_2) \rangle$ decays on times $|t_1 - t_2| \lesssim \omega_r^{-1}$. For $t \gg \omega_r^{-1}$ the phase difference then displays a diffusion-type behavior, with

$$\delta\varphi_{21}^2(t) \approx 2\Gamma_{\phi} t.$$

The parameter

$$\Gamma_{\phi} = \hbar^{-2} \text{Re} \int_0^{\infty} dt \langle \delta\hat{E}_{21}(t) \delta\hat{E}_{21}(0) \rangle \quad (31)$$

gives the dephasing rate.

It follows from Eq. (31) that, to the second order of perturbation theory, linear in ripplon coordinate terms in $\delta\hat{E}_{21}$ give $\Gamma_{\phi} = 0$. The value of Γ_{ϕ} is determined in this approximation by the two-riplon coupling

$$H_i^{(\text{qe})} = \sum_{j=1,2} \sum_{\mathbf{q}, \mathbf{q}'} v_{\mathbf{q}\mathbf{q}'} b_{\mathbf{q}}^{\dagger} b_{\mathbf{q}'}. \quad (32)$$

The individual terms in the sum over \mathbf{q}, \mathbf{q}' describe scattering of a ripplon with wave vector \mathbf{q}' into a ripplon with wave vector \mathbf{q} . The momentum is transferred to the electron and no transitions between electron states occur.

For coupling (32) dephasing rate (31) has the form

$$\Gamma_{\phi} = \frac{\pi}{\hbar^2} \sum_{\mathbf{q}, \mathbf{q}'} |v_{\mathbf{q}\mathbf{q}'1} - v_{\mathbf{q}\mathbf{q}'2}|^2 \bar{n}(\omega_{\mathbf{q}}) [\bar{n}(\omega_{\mathbf{q}'} + 1)] \delta(\omega_{\mathbf{q}} - \omega_{\mathbf{q}'}), \quad (33)$$

where $\bar{n}(\omega) = [\exp(\hbar\omega/k_B T) - 1]^{-1}$ is the Planck number. It is seen from Eq. (33) that only thermally excited riplons with $\omega_{\mathbf{q}} \lesssim k_B T/\hbar$ contribute to the rate Γ_{ϕ} . In what follows we will estimate contributions to Γ_{ϕ} from different mechanisms of electron-riplon coupling taken separately and will again ignore cross terms, which contain products of coupling constants for different mechanisms.

A. Dephasing rate for different coupling mechanisms

The matrix elements $v_{\mathbf{q}\mathbf{q}'j}$ in expression (33) for the dephasing rate are linear in the parameters of the direct two-riplon coupling $H_i^{(2)}$ (11). However, in the second order of perturbation theory they are renormalized by the one-riplon coupling $H_i^{(1)}$ (9),

$$\begin{aligned} v_{\mathbf{q}\mathbf{q}'j} &\approx \frac{\hbar(qq')^{1/2}}{S\rho(\omega_{\mathbf{q}}\omega_{\mathbf{q}'})^{1/2}} \left[\langle j,0,0 | \hat{V}_{-\mathbf{q}\mathbf{q}'} | j,0,0 \rangle e^{-(\mathbf{q}-\mathbf{q}')^2 a_{\parallel}^2/4} \right. \\ &\quad \left. - \sum_{\nu>0, m_{\nu}} (\mathcal{V}_{\mathbf{q}\mathbf{q}'}^{j\nu m_{\nu}} + \mathcal{V}_{-\mathbf{q}'-\mathbf{q}}^{j\nu m_{\nu}}) (\hbar\nu\omega_{\parallel})^{-1} \right], \end{aligned} \quad (34)$$

where $\mathcal{V}_{\mathbf{q}\mathbf{q}'}^{j\nu m_{\nu}} = V_{\mathbf{q}}^{j\nu m_{\nu}} (V_{\mathbf{q}'}^{j\nu m_{\nu}})^*$ and $V_{\mathbf{q}}^{j\nu m_{\nu}} = \langle j,0,0 | \hat{V}_{-\mathbf{q}} e^{-i\mathbf{q}\mathbf{r}} | j, \nu, m_{\nu} \rangle$. In calculating the renormalization due to one-riplon coupling we disregarded the contribution from virtual transitions into different states of out-of-plane motion $|j'\rangle$, because they involve a large energy change (it is straightforward to incorporate the corresponding terms). We also disregarded ripplon energies $\hbar\omega_{\mathbf{q}}$ compared to $\hbar\omega_{\parallel}$.

The contribution $\Gamma_{\phi}^{(k)}$ to the dephasing rate (33) from the direct two-riplon kinematic coupling (12) has a simple form in the case of $\omega_r \ll k_B T/\hbar$. Then $\Gamma_{\phi}^{(k)}$ is determined primarily by forward scattering of riplons off the electron, with $|\mathbf{q} - \mathbf{q}'| \leq 1/a_{\parallel}$, but with $\omega_{\mathbf{q}} = \omega_{\mathbf{q}'} \sim k_B T/\hbar \gg \omega_r$. Calculating the integral over the angle between \mathbf{q} and \mathbf{q}' by the steepest descent method, we obtain

$$\Gamma_{\phi}^{(k)} = \frac{\pi^{1/2} \rho}{27\sqrt{2}a_{\parallel}} \left(\frac{k_B T}{\hbar\sigma} \right)^3 R^2 \bar{K}_{12}^2, \quad (35)$$

where \bar{K}_{12} is the difference of the expectation values of the kinetic energy $p_z^2/2m$ in the states 1 and 2 divided by R . For $E_{\perp} = 0$ we have $\bar{K}_{12} = 3/4$, and one can show that \bar{K}_{12} decreases with increasing E_{\perp} . The numerical value of $\Gamma_{\phi}^{(k)}$ is $\Gamma_{\phi}^{(k)} \leq 0.7 \times 10^2 \text{ s}^{-1}$ for $T = 10 \text{ mK}$ and $\omega_{\parallel}/2\pi = 20 \text{ GHz}$.

The contribution from the direct two-riplon polarization coupling (13) can be estimated by utilizing the fact that the wave vectors of thermal riplons $q_T = (\rho/\sigma)^{1/3} (k_B T/\hbar)^{2/3}$ are less than $1/r_B$ for low temperatures. To lowest order in $q_T r_B$ the polarization contribution is again given by Eq. (35), but now \bar{K}_{12} is the difference of the expectation values of the potential energy $\Lambda/2z$ divided by R . The corresponding rate is of the same order as $\Gamma_{\phi}^{(k)}$.

We now estimate the dephasing rate Γ_{ϕ} (33) due to one-riplon coupling (10). We note first that the kinematic terms in Eq. (10) drop out of the matrix elements $v_{\mathbf{q}\mathbf{q}'j}$,

because they do not have diagonal matrix elements on the functions $|1\rangle, |2\rangle$. The terms quadratic in the electric field E_\perp drop out from the difference $v_{\mathbf{q}\mathbf{q}'1} - v_{\mathbf{q}\mathbf{q}'2}$, because they are independent of the electron state normal to the surface. The major contribution to the dephasing rate comes from the polarization one-rippion coupling $\propto v_{\text{pol}}$ in $\hat{V}_{\mathbf{q}}$ (10). We will denote it as $\Gamma_\phi^{(\text{pol})}$.

The polarization term in $\hat{V}_{\mathbf{q}}$ does not depend on the in-plane electron coordinate. This makes it possible to calculate the sum over ν, m_ν in Eq. (34) for $v_{\mathbf{q}\mathbf{q}'j}$. We will use the relation

$$\begin{aligned} & \sum_{m_\nu} \langle 0,0 | e^{-i\mathbf{q}'\mathbf{r}} | \nu, m_\nu \rangle \langle \nu, m_\nu | e^{i\mathbf{q}\mathbf{r}} | 0,0 \rangle \\ &= \frac{1}{\nu!} (\mathbf{q}\mathbf{q}' a_\parallel^2/2)^\nu \exp[-(q^2 + q'^2) a_\parallel^2/4]. \end{aligned}$$

Further calculation is simplified in the case of $k_B T \gg \omega_r$. Here, again, the major contribution to the dephasing rate comes from forward scattering with $q, q' \gg |\mathbf{q} - \mathbf{q}'|$ and $\mathbf{q}\mathbf{q}' \gg a_\parallel^{-2}$. Then

$$\begin{aligned} & \sum_{\nu \geq 0} \mathcal{V}_{\mathbf{q}\mathbf{q}'}^{j\nu m_\nu} / \hbar \nu \omega_\parallel \approx 2 \langle j | \hat{V}_{-\mathbf{q}} | j \rangle \langle j | \hat{V}_{\mathbf{q}'} | j \rangle \\ & \times \exp[-(\mathbf{q} - \mathbf{q}')^2 a_\parallel^2/4] (\hbar \omega_\parallel a_\parallel^2 q q')^{-1}. \end{aligned}$$

In this approximation we obtain

$$\Gamma_\phi^{(\text{pol})} \sim \frac{\rho}{a_\parallel} \left(\frac{k_B T}{\hbar \sigma} \right)^3 R^2 k_{12}^2,$$

$$k_{12} = |\langle 1 | v_{\text{pol}}(qz) | 1 \rangle|^2 - |\langle 2 | v_{\text{pol}}(qz) | 2 \rangle|^2. \quad (36)$$

The matrix element k_{12} here has to be calculated for $q = q_T$, and we assumed that k_{12} is a smooth function of q for $q \sim q_T$. The numerical value of k_{12} is ≈ 0.23 for $q \approx q_T$ and $T = 10$ mK, it weakly depends on the pressing field E_\perp . The phase relaxation rate from one-rippion polarization coupling is $\Gamma_\phi^{(\text{pol})} \sim 10^2 \text{ s}^{-1}$.

The overall ripplon-induced phase relaxation rate appears to be small. It displays an unusual temperature dependence $\Gamma_\phi \propto T^3$, as seen from Eqs. (35) and (36), and comparatively weakly depends on the in-plane frequency ω_\parallel . We note that it is much smaller than our previous estimate¹⁵ obtained for the case where the in-plane confinement was due to a magnetic field and electrostatic in-plane confinement was comparatively weak.

V. RIPPLON-INDUCED SIDEBAND ABSORPTION

Coupling to ripples modifies the spectrum of microwave absorption by a confined electron. Without this coupling the spectrum would have a δ -shape peak at the transition frequency $(E_2 - E_1)/\hbar$. Ripples lead to a polaronic shift and broadening of the peak. The half-width of the peak Γ_0 is given by the sum of the electron decay and dephasing rates. We will call this spectral peak the zero-rippion line in anal-

ogy with zero-phonon lines in light absorption spectra in solids.

An important consequence of coupling to ripples is also the occurrence of comparatively broad sidebands in the absorption spectrum next to the zero-rippion line. The sidebands are formed, because a microwave-induced electron $|1,0,0\rangle \rightarrow |2,0,0\rangle$ transition can be accompanied by creation or annihilation of one or several ripples. They are similar to phonon sidebands in absorption spectra of defects in solids.³⁷

The ripplon sidebands can be understood from the Franck-Condon picture of a microwave-induced electron transition as happening for an instantaneous ripplon configuration. Since the equilibrium ripplon positions are different in the ground and excited electron states, the transition is accompanied by excitation or absorption of ripples, and the transition energy differs from its value $E_2 - E_1$ in the absence of coupling to ripples.

In order to describe the effect it suffices to keep in the Hamiltonian of the electron-rippion coupling only those terms that have diagonal matrix elements on the electron wave functions $|j,0,0\rangle$, i.e. to replace H_i with

$$\sum_j \langle j,0,0 | H_i | j,0,0 \rangle | j,0,0 \rangle \langle j,0,0 |.$$

One can then apply a standard canonical transformation which shifts ripplon coordinates so that they are counted off from their equilibrium values in the ground electron state. The transformed one-rippion interaction Hamiltonian (9) and (10) then takes a Franck-Condon form

$$H_i^{\text{FC}} = \sum_{\mathbf{q}} \xi_{\mathbf{q}} \Lambda F(q) | 2,0,0 \rangle \langle 2,0,0 |,$$

$$F(q) = q^2 [\langle 2 | v_{\text{pol}}(qz) | 2 \rangle - \langle 1 | v_{\text{pol}}(qz) | 1 \rangle] e^{-q^2 a_\parallel^2/4}. \quad (37)$$

For weak coupling, of primary interest are one-rippion sidebands. Because ripplon occupation numbers are large for $k_B T \gg \hbar \omega_r$, the probabilities of microwave-induced electron transitions accompanied by absorption and emission of a ripplon are the same. Respectively, the sidebands are symmetrical as functions of frequency detuning $\Delta\omega = \omega - (E_2 - E_1)/\hbar$ (we have $|\Delta\omega| \sim \omega_r \ll (E_2 - E_1)/\hbar$). Microwave absorption in the region of the sidebands is quadratic in the electron-rippion coupling parameters. It can be calculated by perturbation theory in H_i^{FC} . From Eq. (37) we obtain for the scaled sideband absorption coefficient $\alpha_{\text{sb}}(\omega)$,

$$\alpha_{\text{sb}}(\omega) = G_{\text{sb}} \bar{\alpha}_{\text{sb}}(\omega), \quad G_{\text{sb}} = \frac{k_B T R^2 r_B^2 \rho}{\pi \hbar^2 \sigma^2 a_\parallel},$$

$$\bar{\alpha}_{\text{sb}} = a_\parallel \int dq q^{-4} F^2(q) \delta(\Delta\omega \pm \omega_q). \quad (38)$$

The absorption coefficient itself is given by α_{sb} multiplied by the integral intensity of the electron absorption spectrum. The latter is the integral of the absorption coefficient over frequency and is equal to the appropriately scaled oscillator strength of the electron transition.

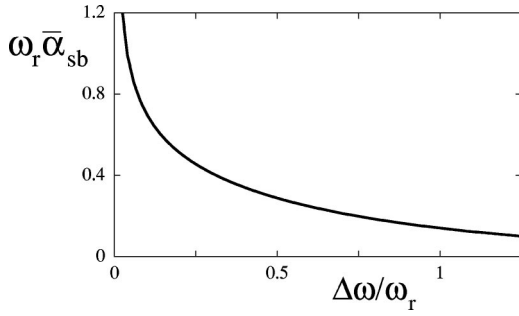


FIG. 5. The scaled coefficient of microwave absorption in the sideband region $\bar{\alpha}_{sb}$ (38) vs frequency detuning $\Delta\omega = \omega - (E_2 - E_1)/\hbar$ for $E_{\perp} = 0$ and $\omega_{\parallel}/2\pi = 20$ GHz.

In Eq. (38) we assumed that $|\Delta\omega|$ is much larger than the half-width of the zero-rippylon line Γ_0 . This condition is satisfied in the interesting region $|\Delta\omega| \sim \omega_r$, since from the above estimates $\omega_r/\Gamma_0 \approx 10^4$.

The sideband intensity is determined by the factor G_{sb} . For $T = 10$ mK and $\omega_{\parallel}/2\pi = 20$ GHz we have $G_{sb} \approx 0.1$. The smallness of G_{sb} indicates that the sidebands formed by two- or many-rippylon processes are not important.

The scaled absorption coefficient in the one-rippylon sideband is shown in Fig. 5. It monotonically decreases with the increasing distance $|\Delta\omega|$ from the zero-rippylon line. For small $|\Delta\omega|$ (but $|\Delta\omega| \gg \Gamma_0$) we have $\bar{\alpha}_{sb} \propto |\Delta\omega|^{-1/3}$. As expected, decay of the sideband absorption with increasing $|\Delta\omega|$ is much slower than decay of the Lorentzian tail of the zero-rippylon line $\propto \Gamma_0/(\Delta\omega)^2$. For large $|\Delta\omega|/\omega_r$, the sideband absorption falls off as $\exp[-(|\Delta\omega|/\omega_r)^{4/3}/2]$, because coupling to short-wavelength riplons is exponentially weak. We note that the one-rippylon sidebands do not display structure, in contrast to sidebands in electron-phonon systems in solids that reflect singularities in the phonon density of states.

A. Intensity of the zero-rippylon line

The integral intensity of the electron absorption spectrum (the oscillator strength) is independent of the electron-rippylon coupling. However, the integral intensity of the zero-rippylon line is reduced by the coupling, because of the sidebands. This reduction is described by a Debye-Waller-type factor (the Pekar-Huang-Reese factor in the theory of electron-phonon spectra) $\exp(-W)$. The parameter W is given by the integral of α_{sb} over ω ,

$$W = G_{sb} \bar{W}, \quad \bar{W} = 2a_{\parallel} \int dq q^{-4} F^2(q). \quad (39)$$

The dependence of the scaling factor \bar{W} on the field E_{\perp} and ω_{\parallel} is shown in Fig. 6. It is clear from this figure and Eq. (39) that W weakly depends on the in-plane electron frequency ω_{\parallel} as long as the corresponding ripplon frequency $\omega_r \ll k_B T/\hbar$. At the same time, W decreases with the increasing pressing field E_{\perp} , because the difference in the effective

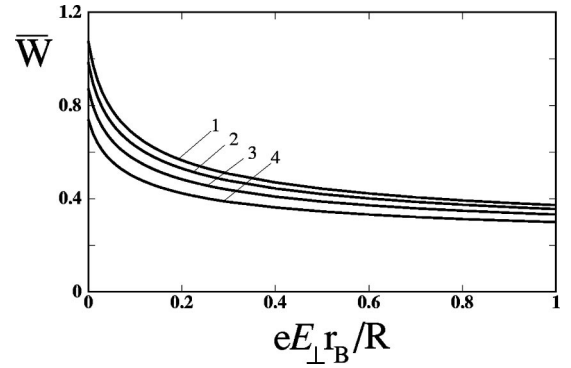


FIG. 6. The scaling factor \bar{W} in expression (39) for the Debye-Waller exponent W . The curves 1 to 4 refer to $r_B/a_{\parallel} = 0.18, 0.25, 0.35, 0.5$ ($\omega_{\parallel}/2\pi \approx 10, 20, 39, 79$ GHz, respectively).

radii of the electron states $|1\rangle$ and $|2\rangle$ decreases, and so does the difference in the ripplon equilibrium positions in the states $|1\rangle$ and $|2\rangle$.

The calculated value of the Debye-Waller factor for electrostatically confined electrons is $W \approx 0.1 - 0.05$ for $\omega_{\parallel}/2\pi = 20$ GHz and E_{\perp} varying from 0 to ~ 300 V/cm. It is close to the estimate $W \sim 0.05$ given earlier¹⁵ for the case of in-plane confinement by a magnetic field. This factor emerges also in the analysis of the operation of a quantum computer based on trapped atomic ions,³⁸ because optical transitions are connected to vibrational modes of the ions (the number of such modes is small, for a small number of ions).

In the context of quantum computing, sideband absorption and the Debye-Waller reduction of the zero-rippylon absorption strength differ qualitatively from electron decay and dephasing. Sideband absorption does not affect an electron qubit between quantum operations. In contrast to dissipative effects, it does not happen between operations. However, it shows that a fraction of electron transitions may go wrong, as they are accompanied by excitation of riplons. Therefore, the Debye-Waller factor characterizes fidelity of quantum operations. The number of “wrong” transitions, and therefore the role of the Debye-Waller factor, depends on the way a specific operation is performed. For example, it depends on the spectral width of a microwave pulse. Optimal ways of performing quantum operations in the presence of sideband absorption will be discussed in a separate publication.

VI. DECAY AND DEPHASING FROM COUPLING TO THE ELECTRODE

Relaxation of a confined electron (qubit) may result also from coupling to the underlying electrode. The corresponding relaxation parameters can be found in the same way as in the case of coupling to riplons/phonons. Fluctuations of the electrode potential modulate the interlevel distance and thus give rise to dephasing. In addition, an electron can make a transition between the states, with energy being transferred to an excitation in the electrode (for example, an electron-hole pair or a plasmon).

The analysis of the dissipation can be formulated in fairly general terms using the fact that the size of the wave function

of the qubit $\sim r_B$ is small compared to the distance to the electrode h . Then the interaction with the electrode can be described in the dipolar approximation,

$$H_{\text{dip}} = -e \delta \hat{\mathcal{E}}_{\perp} z, \quad (40)$$

where $\delta \hat{\mathcal{E}}_{\perp}$ is the fluctuating part of the field on the electron normal to helium surface. This field comes from charge-density fluctuations in the electrode. Equation (40) is just the linear in z/h term in the expansion of the Coulomb coupling energy of the electron and the charge density in the electrode (retardation effects are not important for the frequencies of interest). The field $\delta \hat{\mathcal{E}}_{\perp}$ is an operator with respect to the electrode charge density. Here and below we do not consider effects of fluctuations of the electrode potential on in-plane electron motion; they are weak and less important for qubit dynamics.

Electron relaxation parameters can be expressed in terms of the correlation function of the fluctuating field

$$Q(\omega) = \int_0^{\infty} dt e^{i\omega t} \langle \delta \hat{\mathcal{E}}_{\perp}(t) \delta \hat{\mathcal{E}}_{\perp}(0) \rangle. \quad (41)$$

As we will see, of interest is the behavior of the function $Q(\omega)$ in two frequency regions: low frequencies $\omega \lesssim k_B T / \hbar$ and comparatively high frequencies $\omega \approx (E_2 - E_1) / \hbar$. We will assume that $Q(\omega)$ is smooth in the both regions.

We will consider first the effect of the fluctuations of the electric field with frequencies $\omega \ll (E_2 - E_1) / \hbar$. Such fluctuations result in loss of coherence of the electron states, i.e. dephasing. The dephasing rate can be found in the same way as it was done in Sec. IV for a fluctuating ripplon field. Through linear Stark effect, a slowly varying field $\delta \hat{\mathcal{E}}_{\perp}(t)$ leads to an instantaneous change $\delta \hat{E}_{21}$ of the distance between the electron energy levels E_2 and E_1 . From Eq. (40),

$$\delta \hat{E}_{21}(t) = -e(z_{22} - z_{11}) \delta \hat{\mathcal{E}}_{\perp}(t). \quad (42)$$

A random change of the interlevel distance causes diffusion of the phase difference $\delta \hat{\phi}_{21}(t)$ of the wave functions $|2\rangle$ and $|1\rangle$. As explained in Sec. IV, diffusion behavior is displayed on times that largely exceed the correlation time of the field $\delta \hat{\mathcal{E}}_{\perp}(t)$. The corresponding dephasing rate of the qubit $\Gamma_{\phi}^{(\text{el})}$ is equal to the phase diffusion coefficient. From Eqs. (31), (42) we obtain

$$\Gamma_{\phi}^{(\text{el})} = e^2 (z_{22} - z_{11})^2 \text{Re } Q(0) / \hbar^2. \quad (43)$$

The assumption of a short correlation time of $\delta \hat{\mathcal{E}}_{\perp}(t)$ is equivalent to the assumption that the spectrum $\text{Re } Q(\omega)$ (41) is smooth at frequencies $\omega \lesssim \Gamma_{\phi}^{(\text{el})}$. If this is not the case or if the noise $\delta \hat{\mathcal{E}}_{\perp}(t)$ is non-Gaussian, decay of coherence of the states $|2\rangle$ and $|1\rangle$ becomes nonexponential. Although the analysis has then to be modified, Eq. (42) is still advantageous as it relates dephasing to fluctuations of the field $\delta \hat{\mathcal{E}}_{\perp}(t)$, which can be independently characterized.

The decay rate of the qubit $\Gamma_{12}^{(\text{el})}$ is determined by the probability of a field-induced transition $|2\rangle \rightarrow |1\rangle$ between the electron states. This probability is determined, in turn, by quantum fluctuations of the field $\delta \hat{\mathcal{E}}_{\perp}(t)$ at frequency $\Omega_{12} = (E_2 - E_1) / \hbar$. To the lowest order in the coupling H_{dip} ,

$$\Gamma_{12}^{(\text{el})} = e^2 |z_{12}|^2 \text{Re } Q(\Omega_{12}) / \hbar^2. \quad (44)$$

Here we assumed that decay is due to spontaneous emission only, i.e. that there are no induced processes with energy transfer $E_2 - E_1$.

To estimate relaxation parameters of electrons on helium we will assume that the controlling electrode is a conducting sphere of a small radius r_{el} submerged at depth h beneath helium surface, as discussed in Sec. II. For low frequencies the surface of the sphere is equipotential. Then the fluctuating field of the electrode is simply related to its fluctuating potential $\delta \hat{V}_{\text{el}}$, $\delta \hat{\mathcal{E}}_{\perp} = \delta \hat{V}_{\text{el}} r_{\text{el}} / h^2$.

Much of the low-frequency fluctuations is due to voltage noise from an external lead attached to the electrode. The lead temperature T_{ext} may largely exceed the helium temperature in the cryostat T . The voltage noise is white for $\omega \ll k_B T_{\text{ext}} / \hbar$. Its intensity is given by Nyquist's theorem and is determined by the lead resistance \mathcal{R}_{ext} . From Eq. (43), the dephasing rate is

$$\Gamma_{\phi}^{(\text{el})} = 2k_B T_{\text{ext}} \mathcal{R}_{\text{ext}} e^2 (z_{22} - z_{11})^2 r_{\text{el}}^2 / \hbar^2 h^4. \quad (45)$$

For $\mathcal{R}_{\text{ext}} = 25 \Omega$, $T_{\text{ext}} = 1 \text{ K}$, $r_{\text{el}} = 0.1 \mu\text{m}$, $h = 0.5 \mu\text{m}$, and $z_{22} - z_{11} = r_B$ we obtain $\Gamma_{\phi}^{(\text{el})} \approx 1 \times 10^4 \text{ s}^{-1}$. This shows that thermal electrode noise may be a major source of dephasing for a qubit. Equation (45) indicates how to reduce the dephasing rate. It can be accomplished by further cooling down external leads, reducing their resistance, and increasing the depth by which controlling electrodes are submerged below helium surface.

In contrast to low-frequency noise, high-frequency voltage fluctuations from sources outside the thermostat can be filtered out. Much of high-frequency quantum fluctuations that affect a qubit come from the underlying microelectrode itself. They depend on the interrelation between the electron relaxation time τ_{el} in the electrode and Ω_{12}^{-1} . If $\tau_{\text{el}} \Omega_{12} \ll 1$, the electrode conductivity does not display dispersion up to frequencies $\approx \Omega_{12}$; it greatly exceeds Ω_{12} for typical Ω_{12} .

An order-of-magnitude estimate of the decay rate $\Gamma_{12}^{(\text{el})}$ can be made by assuming that the controlling electrode is a lead attached to a sphere, and this sphere is equipotential (fluctuations of the total charge in the sphere make a major contribution to the field $\delta \hat{\mathcal{E}}_{\perp}$ for small r_{el}/h). Then from Nyquist's theorem

$$\Gamma_{12}^{(\text{el})} = 2(E_2 - E_1) \mathcal{R}_{\text{el}} e^2 |z_{12}|^2 r_{\text{el}}^2 / \hbar^2 h^4, \quad (46)$$

where \mathcal{R}_{el} is the resistance of the lead. If we estimate it as 0.1Ω , then using the same parameters as in the estimate of $\Gamma_{\phi}^{(\text{el})}$ and setting $E_2 - E_1$ equal to the "Rydberg" energy R (1), we obtain $\Gamma_{12}^{(\text{el})} \sim 5 \times 10^2 \text{ s}^{-1}$. Even though this estimate is very approximate, it is clear that the major effect of electrodes on qubit relaxation is dephasing rather than decay.

VII. CONCLUSIONS

In this paper we have provided a comprehensive analysis of parameters of qubits based on electrons on helium. We introduced a simple realistic model of electrodes, which are submerged into helium in order to localize and control the electrons. This model allowed us to estimate parameters of the electron energy spectrum and their dependence on the electrode potential. Control of the qubits is performed by varying the field E_{\perp} normal to helium surface. The field changes the distance between the energy levels of a qubit, which are the ground and first-excited levels of motion normal to the surface. It enables tuning qubits in resonance with each other and with externally applied microwave radiation.

The electrode potential determines not only E_{\perp} , but also the in-plane electron confinement. We found the frequency ω_{\parallel} of electron vibrations parallel to the helium surface and related it to the field E_{\perp} . Typical frequencies $\omega_{\parallel}/2\pi$ are of order of a few tens of GHz for typical $E_{\perp} \sim 100\text{--}300$ V/cm. We analyzed both the cases of one electrode and an electrode array, and investigated the effects of electrode geometry, including the interelectrode distance and the depth by which electrodes are submerged into helium.

We identified relaxation mechanisms, estimated decay rates for a confined electron, and found their dependence on control parameters. In contrast to unconfined electrons studied previously, decay is due primarily to electron transitions, in which energy is transferred to two riplons propagating in opposite directions or to a bulk phonon propagating nearly normal to the surface. We found mechanisms of coupling to phonons. In the cases of both ripplon and phonon scattering, helium excitations with comparatively large wave numbers are involved. For different coupling mechanisms we found the dependence of the decay rate on the parameters of a confined electron. The decay rate is essentially independent of temperature, for low temperatures.

The overall decay rate is of order 10^4 s $^{-1}$ for typical ω_{\parallel} . This estimate is obtained assuming that the typical wave numbers of excitations into which an electron may scatter are $\lesssim 10^7$ cm $^{-1}$. We conjecture that coupling to riplons and phonons with much shorter wavelengths is small. Then the decay rate can be significantly decreased by localizing electrons more strongly in the plane. This will lead to a larger level spacing of the in-plane electron vibrations, and therefore helium excitations with higher energies and wave numbers will be required for decay. The localization can be increased electrostatically through electrode design or by applying a magnetic field perpendicular to the helium surface.

The major mechanism of dephasing due to coupling to excitations of the helium is scattering of thermal riplons off an electron. We calculated the scattering rate and showed that it displays an unusual T^3 temperature dependence. The most significant contribution to the dephasing rate comes from processes which involve virtual transitions between electron states. The ripplon-induced dephasing rate is $\sim 10^2$ s $^{-1}$ for typical ω_{\parallel} and $T=10$ mK.

An important mechanism of dephasing is voltage fluctuations of controlling electrodes. The dephasing rate strongly

depends on the source of these fluctuations and also on the depth by which electrodes are submerged into helium. An estimate for Johnson noise from a typical lead connected to an electrode gives dephasing rate $\sim 10^4$ s $^{-1}$. Our results indicate how this rate can be significantly reduced. Quantum fluctuations of the electrode field give rise to decay of the excited electron state. However, the corresponding decay rate is small.

We also analyzed sidebands of the electron absorption spectrum related to electron transitions accompanied by emission or absorption of a ripplon. We found the Debye-Waller factor that describes the intensity of the zero-riplon absorption line. It gives the overall probability of exciting a ripplon in an electron transition induced by a broadband signal, and therefore it characterizes the fidelity of qubit operations. The shape of ripplon sidebands is important for optimizing control pulses in order to achieve maximal fidelity.

The results provide a quantitative basis for using electrons on helium as qubits of a quantum computer. The clock frequency of such computer Ω_{QC} is determined by the dipole-dipole interelectron interaction and is in the range of $10^7\text{--}10^8$ Hz even for interelectron distances ≈ 1 μm . It largely exceeds both decay and dephasing rates of a confined electron. Our results suggest ways of further reducing these rates. They show how to choose parameters of the system in an optimal way. Because for electrons on helium $E_2 - E_1 \gg \hbar\omega_{\parallel} \gg \hbar\Omega_{QC} \gg \hbar\Gamma$, there is an extremely broad range where the qubit parameters can be dynamically controlled.

ACKNOWLEDGMENTS

We are grateful to A. Dahm, B. Golding, and J. Goodkind for valuable discussions. This research was supported by the NSF through Grant No. ITR-0085922.

APPENDIX: ONE-RIPPLON POLARONIC EFFECT

Besides relaxation, coupling to riplons leads also to a polaronic effect. Because ripplon frequencies are low, the major contribution comes from processes in which a ripplon is created or annihilated, but the state of the electron system

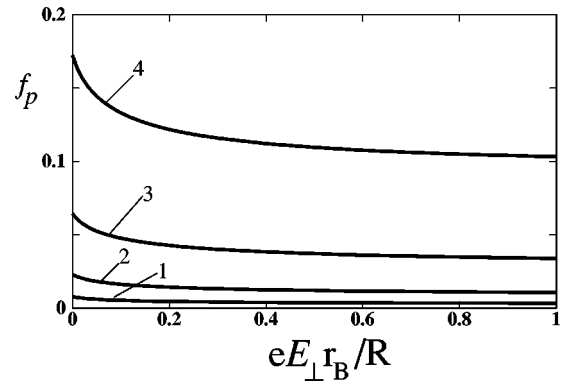


FIG. 7. The factor f_p in the Franck-Condon polaronic shift of the transition frequency of a qubit (A1) as a function of the pressing field E_{\perp} for typical values of the in-plane localization length a_{\parallel} . The curves 1 to 4 correspond to $r_B/a_{\parallel} = 0.18, 0.25, 0.35, 0.5$; the respective values of $\omega_{\parallel}/2\pi$ are $\approx 10, 20, 39, \text{ and } 79$ GHz.

is not changed. Polaronic shift of the electron transition frequency is then determined by the diagonal matrix elements of $H_i^{(1)}$ (9) on the wave functions $|1,0,0\rangle, |2,0,0\rangle$. Keeping only these terms in $H_i^{(1)}$ corresponds to the adiabatic approximation in which riplons have different equilibrium positions depending on the presence of an electron (one can think of a “dimple” made by an electron on helium surface¹⁹) and on the electron state. Of primary interest to us is the state dependence, as it characterizes the strength of coupling of the electron transition to riplons. The corresponding coupling is described by the Franck-Condon interaction Hamiltonian (37).

The Franck-Condon polaronic shift of the transition frequency $1 \rightarrow 2$ due to coupling (37) is given by a simple perturbation theory,

$$P = P_{12} f_p(a_{\parallel}, E_{\perp}), \quad P_{12} = R^2 / 4\pi^2 \hbar \sigma r_B^2, \quad (A1)$$

$$f_p = (4\pi\sigma/\rho) r_B^4 \int_0^{\infty} dq q^2 F^2(q) \omega_q^{-2},$$

where f_p is a dimensionless factor determined by the matrix elements of v_{pol} (10) on the wave functions of out-of-plane motion. It depends on the dimensionless parameters a_{\parallel}/r_B and $eE_{\perp}r_B/R$, and is numerically small for typical parameter values, see Fig. 7.

The numerical value of the factor P_{12} is $P_{12}/2\pi \approx 2.2 \times 10^7$ Hz. The energy $\hbar P_{12}$ is much less than the distance between the electron energy levels. The shift P is also smaller than the typical frequency ω_r of riplons coupled to the electron (28). The inequality $|P| \ll \omega_r$ indicates that the $|1\rangle \rightarrow |2\rangle$ transition is weakly coupled to riplons.

*Electronic address: dykman@pa.msu.edu

¹D. Loss and D.P. DiVincenzo, Phys. Rev. A **57**, 120 (1998).

²A. Imamoglu, D.D. Awschalom, G. Burkard, D.P. DiVincenzo, D. Loss, M. Sherwin, and A. Small, Phys. Rev. Lett. **83**, 4204 (1999).

³R. Vrijen, E. Yablonovitch, K. Wang, H.W. Jiang, A. Balandin, V. Roychowdhury, T. Mor, and D. DiVincenzo, Phys. Rev. A **62**, 012306 (2000).

⁴B.E. Kane, Nature (London) **393**, 133 (1998).

⁵T.D. Ladd, J.R. Goldman, F. Yamaguchi, Y. Yamamoto, E. Abe, and K.M. Itoh, Phys. Rev. Lett. **89**, 017901 (2002).

⁶M.S. Sherwin, A. Imamoglu, and Th. Montroy, Phys. Rev. A **60**, 3508 (1999).

⁷G. Chen, N.H. Bonadeo, D.G. Steel, D. Gammon, D.S. Katzer, D. Park, and L.J. Sham, Science **289**, 1906 (2000).

⁸T.H. Stievater, X.Q. Li, D.G. Steel, D. Gammon, D.S. Katzer, D. Park, C. Piermarocchi, and L.J. Sham, Phys. Rev. Lett. **87**, 133603 (2001).

⁹V.D. Averin, Solid State Commun. **105**, 659 (1998).

¹⁰Y. Nakamura, Yu.A. Pashkin, and H.S. Tsai, Nature (London) **398**, 786 (1999).

¹¹J.R. Friedman, V. Patel, W. Chen, S.K. Tolpygo, and J.E. Lukens, Nature (London) **406**, 43 (2000).

¹²C.H. van der Wal, A.C.J. ter Haar, F.K. Wilhelm, R.N. Schouten, C.J.P.M. Harmans, T.P. Orlando, S. Lloyd, and J.E. Mooij, Science **290**, 773 (2000).

¹³Y. Yu, S. Han, Xi Chu, S.-I. Chu, and Zh. Wang, Science **296**, 889 (2002).

¹⁴D. Vion, A. Aassime, A. Cottet, P. Joyez, H. Pothier, C. Urbina, D. Esteve, and M.H. Devoret, Science **296**, 886 (2002).

¹⁵P.M. Platzman and M.I. Dykman, Science **284**, 1967 (1999).

¹⁶M.I. Dykman and P.M. Platzman, Quantum Inf. Comput. **1**, 102 (2001).

¹⁷K.R. Brown, D.A. Lidar, and K.B. Whaley, Phys. Rev. A **65**, 012307 (2002).

¹⁸D. DeMille, Phys. Rev. Lett. **88**, 067901 (2002).

¹⁹*Two Dimensional Electron Systems on Helium and Other Cryogenic Substrates*, edited by E. Y. Andrei (Kluwer Academic, Dordrecht, MA, 1997).

²⁰K. Shirahama, S. Ito, H. Suto, and K. Kono, J. Low Temp. Phys.

101, 439 (1995).

²¹M.J. Lea, P.G. Frayne, and Yu. Mukharsky, Fortschr. Phys. **48**, 1109 (2000).

²²J.M. Goodkind and S. Pilla, Quantum Inf. Comput. **1**, 108 (2001).

²³A.J. Dahm, J.M. Goodkind, I. Karakurt, and S. Pilla, J. Low Temp. Phys. **126**, 709 (2002).

²⁴In the absence of in-plane confinement, electronic transitions between the states (1) and the Stark shift of the transition frequency were observed using microwave spectroscopy by C.C. Grimes, T.R. Brown, M.L. Burns, and C.L. Zipfel, Phys. Rev. B **13**, 140 (1976).

²⁵E. Cheng, M.W. Cole, and M.H. Cohen, Phys. Rev. B **50**, 1136 (1994).

²⁶M.M. Nieto, Phys. Rev. A **61**, 034901 (2000).

²⁷S.H. Patil, Phys. Rev. A **64**, 064902 (2001).

²⁸M. A. Niesen and I. L. Chuang, *Quantum Computation and Quantum Information* (Cambridge University Press, Cambridge, 2000).

²⁹Recent experimental data on the ⁴He liquid-vapor interface were obtained by K. Penanen, M. Fukuto, R.K. Heilmann, I.F. Silvera, and P.S. Pershan, Phys. Rev. B **62**, 9621 (2000); Quantum Monte Carlo simulations for symmetric helium films were done recently by E.W. Draeger and D.M. Ceperley, Phys. Rev. Lett. **89**, 015301 (2002).

³⁰P.M. Platzman and G. Beni, Phys. Rev. Lett. **36**, 626 (1976).

³¹M. Saitoh, J. Phys. Soc. Jpn. **42**, 201 (1977).

³²Yu.P. Monarkha and V.B. Shikin, Fiz. Nizk. Temp. **8**, 563 (1982) [Sov. J. Low Temp. Phys. **8**, 279 (1982)].

³³M.I. Dykman, Phys. Status Solidi B **88**, 463 (1978).

³⁴Yu.P. Monarkha, Fiz. Nizk. Temp. **4**, 1093 (1978) [Sov. J. Low Temp. Phys. **4**, 515 (1978)].

³⁵D.O. Edwards, J.R. Eckardt, and F.M. Gasparini, Phys. Rev. A **9**, 2070 (1974).

³⁶A. Latri, F. Dalfovo, L. Pitaevskii, and S. Stringari, J. Low Temp. Phys. **98**, 227 (1995).

³⁷W. Hayes and A. M. Stoneham, *Defects and Defect Processes in Nonmetallic Solids* (Wiley, NY, 1985).

³⁸D.J. Wineland, C. Monroe, W.M. Itano, D. Leibfried, B.E. King, and D.M. Meekhof, J. Res. Natl. Inst. Stand. Technol. **103**, 259 (1998).